

Simulation of the Motion of a Five-Link Crawling Robot with Controlled Friction on a Surface Having Obstacles

L. Yu. Vorochaeva*, A. S. Yatsun, and S. F. Yatsun

Southwest State University, Kursk, 305040 Russia

**e-mail: teormeh@inbox.ru*

Received June 22, 2016; in final form, January 27, 2017

Abstract—We consider the motion of a five-link crawling robot in an environment with obstacles located discretely. The robot is fitted with special controlled friction elements for the periodic fixation of links on the surface and has a possibility of the spatial configuration change due to a detachment of the end links from the surface. One of the possible crawling modes is analyzed as the end links are detached from the surface and the adjacent links rotate by a given angle in the plane of motion without interaction with obstacles. As the result of simulating by the numerical method, we establish the dependence between the average velocity of the plant (and its maneuverability between obstacles) and control values.

DOI: 10.1134/S1064230717030133

INTRODUCTION

At present, the number of robots elaborated around principles of the motion of living organisms has been intensively increased. Devices of this kind have proved their efficiency under a variety of operating conditions. Among the distributed types of such devices are crawling robots. They consist most often of several links and hinges that connect them, in which the drives are located [1–12]. Due to such a construction, the links can move relative to each other and implement variations of a gait.

The motion of multilink systems across a horizontal surface, the interaction with which is described by the dry or viscous forces, has received much attention in [13–22]. In these works, the inertial method of motion is considered such that with the slow and fast links' motions relative to the main link it remains stationary and moves in the required direction, respectively [13–18]. In [19], the optimal control of the motion of a multilink system is studied; the system consists of the main body and one or two links connected with it by cylindrical hinges, in a resisting environment whose resistance force depends on the velocity of the links. For the considered system, one estimates the average velocity of its progressive motion and obtains the control laws of oscillation of the links such that the maximum average motion velocity is implemented. In [20], the periodic motion of a flat two-link robot is investigated; the robot is controlled by the intrinsic moment applied to a hinge that connects the links across a horizontal plane with the availability of dry friction. The dynamics of the two-link robot is analyzed (the analysis takes into account the effect of the friction forces and the boundedness of the control moment), the algorithm of the motion of the two-link robot across the plane is proposed (here, the straight motion is ensured), and the influence of various geometric and mechanical parameters of the system on the average motion velocity and on the energy costs in the motion of the two-link robot across the plane is studied. The motion of a mechanical system that consists of the main body and one or two links connected with it in a resisting environment is considered in [21]; and the motion is controlled through high-frequency periodic oscillations of the links. The motion equation of this system is derived and the average velocity of the motion is estimated; it is found that this velocity is positive if the angular velocity of the detachment of the attached links is smaller than the angular velocity bringing them to the axis of the body. The research of the controlled motion of flat multilink robots across a horizontal plane with the availability of the dry friction forces obeying the Coulomb law is touched upon in [22]. A multilink robot is controlled by intrinsic moments applied to hinges that connect the adjacent links; methods for control that ensure the motion of a multilink robot in a given direction are developed.

Investigations in this field are also being pursued by other researchers. In [23], multilink mechanisms that simulate the gaits of snakes and worms are considered; their movement is carried out through the

interaction with a support surface by changing the configuration of a mechanism. The control algorithms that allow an operator to control the velocity and the direction of a motion are proposed; here, the change in a mechanism-configuration that implements the desired motion is performed automatically. In [24, 25], the results of researching the dynamics of a snake-like three-link robot (the motion across a rough surface) that can move by changing its geometric configuration are presented.

Another method for moving a three-link robot across a horizontal surface is described in [26–31]. The motion is performed not by inertia, but by the control of dry friction forces exerted between support elements of the central link and the surface. In the interaction of the supports by the contact elements with the large and small friction coefficients, the main link is stationary and moves across the plane, respectively. The mathematical model of the robot motion is constructed; the model describes two possible types of movements of the mechanism (longitudinal and transverse) such that for them two phases alternate, namely, the motion across smooth (the friction coefficient is small and tends to zero) and rough (the friction coefficient is large) surfaces. It is found that such a method of movement allows one to increase the average velocity of the robot motion in relation to the inertia method, because there is no need for slow motion.

The attention of researchers has been drawn in particular to the analysis of the controlled motion of such robots along an assigned trajectory in accordance with the taken mode and the corresponding step-wise movement of the robot's links. Here, one of the main problems consists in increasing the average velocity of the robot's motion; this can be performed through using contact elements (frictional supports) with the controlled coefficient of dry friction that are located on particular links [26–31]. Another important problem is improving the maneuverability of robots that move across a surface with discretely located obstacles; for this purpose, one often uses devices with reconfigurable links whose mutual location depends on the terrain through which the motion is performed [32].

In the present paper, we consider the motion of a five-link crawling robot across a plane with discretely located obstacles, from a certain initial point to a certain end point; the motion is characterized by no interaction of the robot's links with obstacles in the periodic sliding of the central link along the axis of symmetry lying in a horizontal plane and passing through the center of mass of this link normally to it, without its detachment from the surface. Here, the lateral links perform synchronized antiphase rotations and the end links are periodically detached from the surface. In order to increase the average velocity, the construction is equipped by controlled frictional supports, which allow one to change at given instants the friction coefficient at the contact points with the support surface, while in order to improve the maneuverability of the plant, the configuration of the device is changed through the spatial movements of the links relative to each other.

The basic aim of this work is to develop a dynamic mathematical model of a crawling robot; the model represents the sequence of steps associated with the differential motion equations with respect to the imposed connections, the model of the interaction of supports with a surface, and the model of the passage of obstacles, as well as the design of the motion-control system of the device and the study of the influence of the control values on the average velocity and the maneuverability across the surface.

1. DESCRIPTION OF THE ROBOT

We introduce the notion of an environment with obstacles such that a crawling robot moves in it. For such an environment, we consider a horizontal Oxy -plane with discretely located obstacles A , B , etc.; they have the shape of parallelepipeds with dimensions $l_k \times b_k \times h_k$. Their position in the plane depends on the x_k and y_k coordinates along the Ox - and Oy -axes, where k is a letter designation of an obstacle. Figure 1 shows two obstacles A and B , the distance between which is $L_{AB} = \sqrt{x_{AB}^2 + y_{AB}^2}$, where $x_{AB} = |x_A - x_B|$ and $y_{AB} = |y_A - y_B|$.

The considered robot represents a serial chain of five links 1 – 5 (Fig. 2a); links 1 and 2 , along with 4 and 5 , are symmetrically attached relative to the middle (central) link 3 [32]. The links of each adjacent pair are connected together by the hinges equipped with rotary servo drives having integrated reducers (in order to decrease the rotational velocity and increase the generated moment) and sensors of the rotation angle, which allow one to measure the relative angles between the links. Hinges 6 installed between links 1 and 2 and between links 5 and 4 generate moments M_{21} and M_{45} , as well as ensure the rotation of the end links 1 and 5 about the horizontal axes in the vertical planes. Hinges 7 installed at the ends of the middle link 3 generate moments M_{32} and M_{34} , as well as make it possible to rotate adjacent links 2 and 4 about the vertical axes in a horizontal plane.

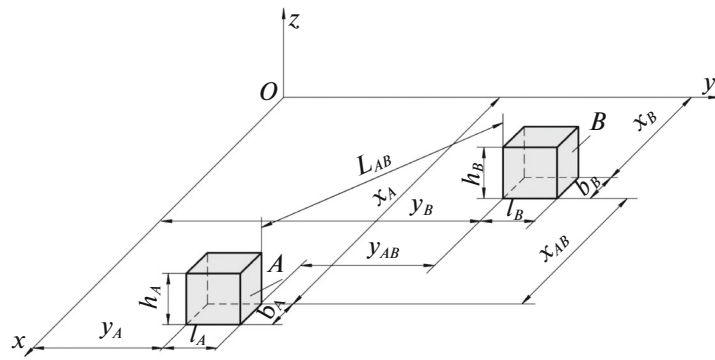


Fig. 1. Environment with discretely located obstacles.

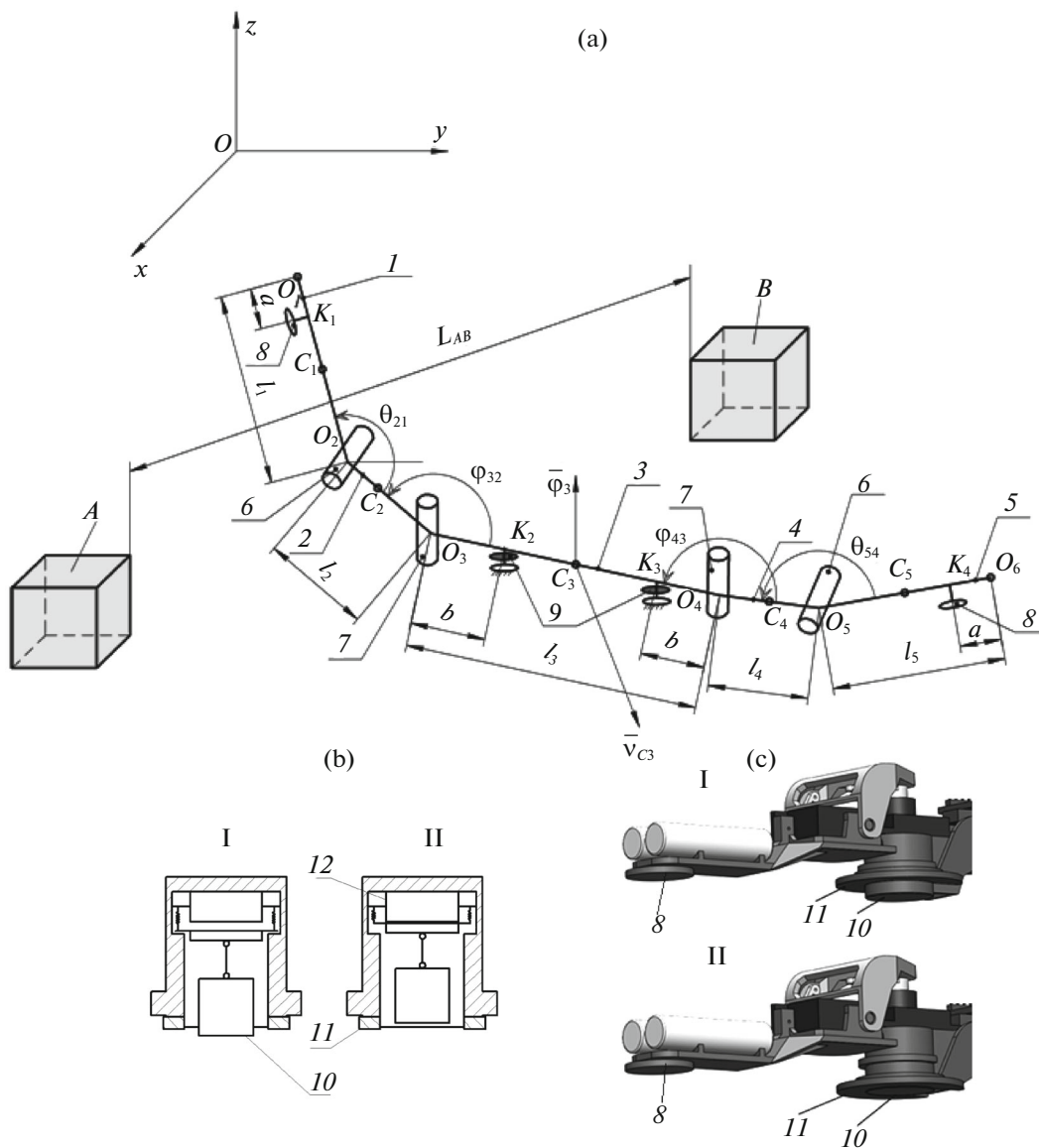


Fig. 2. (a) Diagram of crawling five-link robot; *A* and *B* are obstacles. (b) Diagram of supports of central link. (c) External appearance of support surfaces; I is contact with small friction coefficient and II is contact with large friction coefficient.

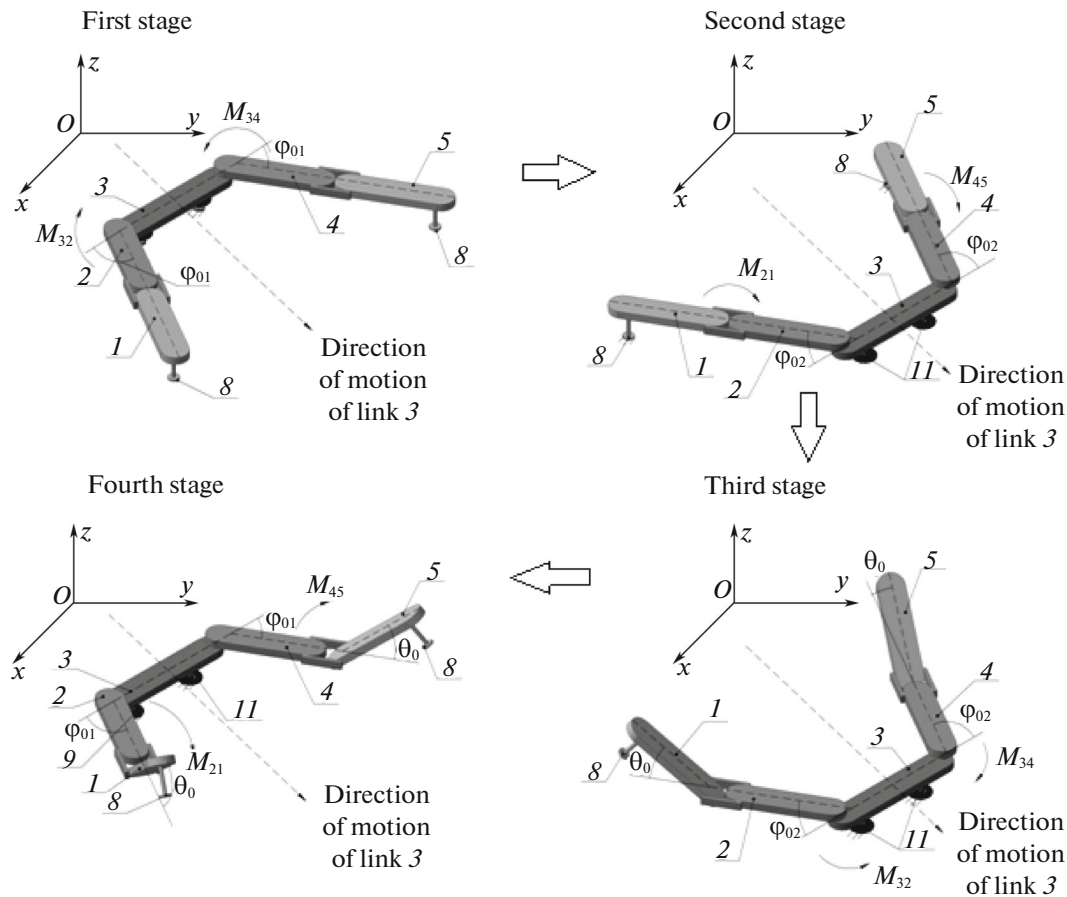


Fig. 3. Stages of robot motion.

Contact of the robot with the surface is enabled through four supports, namely, uncontrolled supports 8 (installed on links 1 and 5) and controlled supports 9 (on link 3). To control the friction coefficient in the interaction of the robot with the surface, supports 9 have the mechanism of varying their frictional properties (anisotropic supports) by replacing support elements 10 and 11 in the contact area with different friction coefficients (Fig. 2b). Support 9 is equipped with a drive of progressive motion 12, which includes an electromagnet and the return springs. The drive makes it possible to move element 10 along the vertical axis; the surface of this element has a small friction coefficient, whereas the surface of element 11 has a large friction coefficient. Figure 2c presents the general view of the controlled supports of the robot. It is clearly seen that support 9 has two contact surfaces, namely, the circle and the ring. The friction coefficient of the surface of the ring is larger than this coefficient of the surface of the circle. The sizes of supports 8 and 9 ensure the stable position of the robot when links 1, 2, 4, and 5 rotate.

The robot moves from the initial position in which links 2 and 4 are located at equal angles φ_{01} relative to link 3, links 1 and 5 interact with the surface, and link 3 comes into contact with the surface by support elements 10. The motion consists of four stages; during each stage certain movements of the links of the robot are performed (Fig. 3).

At the first stage, links 1 and 2, as well as 4 and 5, represent a whole entity and synchronously rotate in antiphase (with respect to the central link), under the action of moments M_{32} and M_{34} until the relative angles become equal to φ_{02} . In turn, due to the interaction with the surface by supports 10 with the small friction coefficient, the central link slides forward; its rotation around the vertical axis is missing. After the completion of the first stage, support surface 10 moves up by drive 12; here, supports 9 come into contact by elements 11 with a large friction coefficient, which provides the fixation of the central link on the surface during the second to fourth stages. At the second stage, links 1 and 5 are detached from the surface by drives 6 due to the rotations with the opposing angular velocities with the use of moments M_{21} and M_{45} through equal angles θ_0 . At the third stage, links 2 and 4, as well as links 1 and 5, which are rigidly con-

nected with them, synchronously rotate in antiphase (with respect to hinges 7) by the corresponding drives (moments M_{32} and M_{34}) until their rotation angles relative to link 3 attain values of φ_{01} . At the fourth stage, links 1 and 5 move down until they are located at identical angles (equal to 0°) with the surface due to drives 6 (moments M_{21} and M_{45}). After the completion of the fourth stage, the support elements 10 at the central link move down by drives 12 until contact with the surface is made. After that, the sequence of stages can be repeated until the robot reaches the required end point.

2. MATHEMATICAL MODEL OF THE ROBOT MOTION

2.1. Kinematic Analysis

The robot motion is considered in the absolute coordinate system $Oxyz$; here, the robot moves across the Oxy -plane. Each link is associated with a relative (local) coordinate system $O_i x_i y_i z_i$ whose $O_i x_i$ -axis is directed along the longitudinal axis of the link. As a result, the $O_i x_i$ - and $O_i y_i$ -axes form with the Oxy - and Oxz -planes angles φ_i and θ_i , respectively (counted counter-clockwise). It is assumed that each i th link of the robot represents an absolutely solid bar $O_i O_{i+1}$ of length l_i and mass m_i ; here, the center of mass of this bar coincides with its center of symmetry (point C_i in Fig. 2a). Support elements 8 are placed at points K_1 and K_4 , which are remote from the ends of links 1 and 5 at distance a , whereas supports 9 are located at points K_2 and K_3 , the distances between which and the end points of link 3 are equal to b .

With the considered mode of motion, links 2–4 always lie in a plane that is parallel to the Oxy -plane and is remote from it at the distance z_{C3} . Links 2 and 4 form with link 3 angles $\varphi_{32} = \varphi_{43}$ and links 1 and 5 form with links 2 and 4 angles $\theta_{21} = \theta_{54}$, respectively. In the general case, link 3 performs a plane-parallel motion, which is characterized by the linear v_{C3} and angular $\dot{\varphi}_3$ velocities.

In the context of kinematic analysis, the problem of the positions is solved; this makes it possible to identify the coordinates of the characteristic points of the mechanism (centers of mass of the links, as well as their end points and contact points) with the known values of the generalized coordinates, i.e., to describe the mode of the robot motion. For this purpose, the rotation matrices are used; the matrix T_{φ_i} is true for links that rotate in the Oxy -plane and the matrix T_{θ_i} is valid for links that rotate in the Oxz -plane:

$$T_{\varphi_i} = \begin{pmatrix} \cos \varphi_i & -\sin \varphi_i & 0 \\ \sin \varphi_i & \cos \varphi_i & 0 \\ 0 & 0 & 1 \end{pmatrix}, \quad i = 2, 3, 4; \quad T_{\theta_i} = \begin{pmatrix} \cos \theta_i & 0 & \sin \theta_i \\ 0 & 1 & 0 \\ -\sin \theta_i & 0 & \cos \theta_i \end{pmatrix}, \quad i = 1, 5.$$

The radius vector of point O_1 is

$$\bar{r}_{O1} = (x_{O1}, y_{O1}, z_{O1})^T.$$

Link 1 can rotate in two planes (at angles φ_2 and θ_1); therefore, to determine the coordinates of the points of this link one uses the rotation matrix T_{10} , which represents the product of two matrices:

$$T_{10} = T_{\varphi_2} T_{\theta_1},$$

$$T_{10} = \begin{pmatrix} \cos \theta_1 \cos \varphi_2 & -\sin \varphi_2 \sin \theta_1 \cos \varphi_2 \\ \cos \theta_1 \sin \varphi_2 & \cos \varphi_2 \sin \theta_1 \sin \varphi_2 \\ -\sin \theta_1 & 0 & \cos \theta_1 \end{pmatrix}.$$

In the general form, the radius vectors of points K_1 , C_1 , and O_2 can be presented as follows:

$$\bar{r}_{K1(C1,O2)} = \bar{r}_{O1} + T_{10} \bar{r}_{O1K1(C1,O2)}^{(1)},$$

where $\bar{r}_{O1K1(C1,O2)}^{(1)} = (l_{O1K1(C1,O2)} \ 0 \ 0)^T$ is the radius vector of point K_1 (C_1 and O_2) about point O_1 in the coordinate system $O_1 x_1 y_1 z_1$, $l_{O1K1} = a$, $l_{O1C1} = l_1/2$, and $l_{O1O2} = l_1$.

The radius vectors of points C_3 and O_3 are presented as follows:

$$\bar{r}_{C3(O3)} = \bar{r}_{O1} + T_{10} \bar{r}_{O1O2}^{(1)} + T_{20} \bar{r}_{O2C3(O3)}^{(2)},$$

where $T_{20} = T_{\theta_1}$, $\bar{r}_{O_2C_3(O_3)}^{(2)} = (l_{O_2C_3(O_3)} \ 0 \ 0)^T$ are the radius vectors of points C_3 and O_3 about point O_2 in the coordinate system $O_2x_2y_2z_2$, $l_{O_2C_3} = l_2/2$, and $l_{O_2O_3} = l_2$.

The radius vectors of points K_2 , K_3 , C_3 , and O_4 are

$$\bar{r}_{K_2(K_3, C_2, O_4)} = \bar{r}_{O_1} + T_{10}\bar{r}_{O_1O_2}^{(1)} + T_{20}\bar{r}_{O_2O_3}^{(2)} + T_{30}\bar{r}_{O_3K_2(K_3, C_2, O_4)}^{(3)},$$

where $T_{30} = T_{\varphi_3}$, $\bar{r}_{O_3K_2(K_3, C_2, O_4)}^{(3)} = (l_{O_3K_2(K_3, C_2, O_4)} \ 0 \ 0)^T$ are the radius vectors of points K_2 (K_3 , C_3 , and O_4) about point O_3 in the coordinate system $O_3x_3y_3z_3$, $l_{O_1K_1} = a$, $l_{O_3K_3} = l_3 - b$, $l_{O_3C_2} = l_3/2$, and $l_{O_3O_4} = l_3$.

The radius vectors of points C_4 and O_5 are presented as follows:

$$\bar{r}_{C_4(O_5)} = \bar{r}_{O_1} + T_{10}\bar{r}_{O_1O_2}^{(1)} + T_{20}\bar{r}_{O_2O_3}^{(2)} + T_{30}\bar{r}_{O_3O_4}^{(3)} + T_{40}\bar{r}_{O_4C_4(O_5)}^{(4)},$$

where $T_{40} = T_{\varphi_4}$ and $\bar{r}_{O_4C_4(O_5)}^{(4)} = (l_{O_4C_4(O_5)} \ 0 \ 0)^T$ are the radius vectors of points C_4 and O_5 about point O_4 in the coordinate system $O_4x_4y_4z_4$, $l_{O_4C_4} = l_4/2$, and $l_{O_4O_5} = l_4$.

In the general form, the radius vectors of points K_4 , C_5 , and O_6 can be presented as follows:

$$\bar{r}_{K_4(C_5, O_6)} = \bar{r}_{O_1} + T_{10}\bar{r}_{O_1O_2}^{(1)} + T_{20}\bar{r}_{O_2O_3}^{(2)} + T_{30}\bar{r}_{O_3O_4}^{(3)} + T_{40}\bar{r}_{O_4O_5}^{(4)} + T_{50}\bar{r}_{O_5K_4(C_5, O_6)}^{(5)},$$

where $T_{50} = T_{\theta_5}$, $\bar{r}_{O_5K_4(C_5, O_6)}^{(5)} = (l_{O_5K_4(C_5, O_6)} \ 0 \ 0)^T$ are the radius vectors of points K_4 (C_5 and O_6) about point O_5 in the coordinate system $O_5x_5y_5z_5$, $l_{O_5K_4} = l_5 - a$, $l_{O_5C_5} = l_5/2$, and $l_{O_5O_6} = l_5$.

Taking into account the connections stemming from the kinematic diagram of the robot and the consideration of the mode of its motion in which the supports of link 3 never detach from the surface and the rotation of this link in a horizontal plane does not occur, the vector of generalized coordinates is presented as follows:

$$\bar{q} = (x_{C_3} \ y_{C_3} \ \theta_1 \ \varphi_2 \ \varphi_4 \ \theta_5)^T.$$

The solution of the problem of velocities allows one to obtain expressions for velocities of the centers of mass of the links of the plant; these expressions are used next in the dynamic analysis when determining the kinetic energies of the links. The velocities of the main points are determined as follows:

$$\begin{aligned} \dot{\bar{r}}_{O_1} &= (\dot{x}_{O_1}, \dot{y}_{O_1}, \dot{z}_{O_1})^T, \\ \dot{\bar{r}}_{K_1(C_1, O_2)} &= \dot{\bar{r}}_{O_1} + \dot{T}_{10}\bar{r}_{O_1K_1(C_1, O_2)}^{(1)}, \\ \dot{\bar{r}}_{C_3(O_3)} &= \dot{\bar{r}}_{O_1} + \dot{T}_{10}\bar{r}_{O_1O_2}^{(1)} + \dot{T}_{20}\bar{r}_{O_2C_3(O_3)}^{(2)}, \\ \dot{\bar{r}}_{K_2(K_3, C_2, O_4)} &= \dot{\bar{r}}_{O_1} + \dot{T}_{10}\bar{r}_{O_1O_2}^{(1)} + \dot{T}_{20}\bar{r}_{O_2O_3}^{(2)} + \dot{T}_{30}\bar{r}_{O_3K_2(K_3, C_2, O_4)}^{(3)}, \\ \dot{\bar{r}}_{C_4(O_5)} &= \dot{\bar{r}}_{O_1} + \dot{T}_{10}\bar{r}_{O_1O_2}^{(1)} + \dot{T}_{20}\bar{r}_{O_2O_3}^{(2)} + \dot{T}_{30}\bar{r}_{O_3O_4}^{(3)} + \dot{T}_{40}\bar{r}_{O_4C_4(O_5)}^{(4)}, \\ \dot{\bar{r}}_{K_4(C_5, O_6)} &= \dot{\bar{r}}_{O_1} + \dot{T}_{10}\bar{r}_{O_1O_2}^{(1)} + \dot{T}_{20}\bar{r}_{O_2O_3}^{(2)} + \dot{T}_{30}\bar{r}_{O_3O_4}^{(3)} + \dot{T}_{40}\bar{r}_{O_4O_5}^{(4)} + \dot{T}_{50}\bar{r}_{O_5K_4(C_5, O_6)}^{(5)}, \end{aligned}$$

where \dot{T}_{10} , \dot{T}_{20} , \dot{T}_{30} , \dot{T}_{40} , and \dot{T}_{50} are derivatives of the corresponding rotation matrices.

The problem of accelerations is core to obtain the formulas by which the accelerations of the centers of mass of the links of the device are determined; this also finds application in the dynamic analysis when determining time derivatives of the kinetic energies of links. The accelerations of the main points are determined as follows:

$$\begin{aligned} \ddot{\bar{r}}_{O_1} &= (\ddot{x}_{O_1}, \ddot{y}_{O_1}, \ddot{z}_{O_1})^T, \\ \ddot{\bar{r}}_{K_1(C_1, O_2)} &= \ddot{\bar{r}}_{O_1} + \ddot{T}_{10}\bar{r}_{O_1K_1(C_1, O_2)}^{(1)}, \\ \ddot{\bar{r}}_{C_3(O_3)} &= \ddot{\bar{r}}_{O_1} + \ddot{T}_{10}\bar{r}_{O_1O_2}^{(1)} + \ddot{T}_{20}\bar{r}_{O_2C_3(O_3)}^{(2)}, \\ \ddot{\bar{r}}_{K_2(K_3, C_2, O_4)} &= \ddot{\bar{r}}_{O_1} + \ddot{T}_{10}\bar{r}_{O_1O_2}^{(1)} + \ddot{T}_{20}\bar{r}_{O_2O_3}^{(2)} + \ddot{T}_{30}\bar{r}_{O_3K_2(K_3, C_2, O_4)}^{(3)}, \\ \ddot{\bar{r}}_{C_4(O_5)} &= \ddot{\bar{r}}_{O_1} + \ddot{T}_{10}\bar{r}_{O_1O_2}^{(1)} + \ddot{T}_{20}\bar{r}_{O_2O_3}^{(2)} + \ddot{T}_{30}\bar{r}_{O_3O_4}^{(3)} + \ddot{T}_{40}\bar{r}_{O_4C_4(O_5)}^{(4)}, \end{aligned}$$

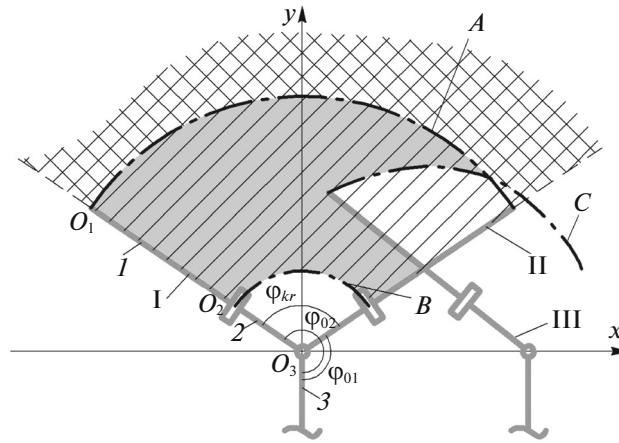


Fig. 4. Diagram of operating areas of links.

$$\ddot{\vec{r}}_{K4(C5,O6)} = \ddot{\vec{r}}_{O1} + \ddot{T}_{10} \vec{r}_{O1O2}^{(1)} + \ddot{T}_{20} \vec{r}_{O2O3}^{(2)} + \ddot{T}_{30} \vec{r}_{O3O4}^{(3)} + \ddot{T}_{40} \vec{r}_{O4O5}^{(4)} + \ddot{T}_{50} \vec{r}_{O5K4(C5,O6)}^{(5)},$$

where \ddot{T}_{10} , \ddot{T}_{20} , \ddot{T}_{30} , \ddot{T}_{40} , and \ddot{T}_{50} are second derivatives of the corresponding rotation matrices.

2.2. Model of Passage between Obstacles



The considered mode of the robot motion across a horizontal surface in the absence of detachments of links 1 and 5 from the surface for changing the configuration of the device can be reduced to a flat transverse gait; this is detailed in [26–28]. Such a plane motion can be used in order to move the robot across a surface without obstacles (in free space). However, with discretely located obstacles in the path of the robot, it is necessary to improve its maneuverability. By the maneuverability, here, we mean the ratio of the largest transversal size of the robot



$$L = \sum_{i=1}^5 l_i$$

to the minimum distance between obstacles L_{ABmin} : $\xi = L/L_{ABmin}$. For their contactless passage, the largest transversal size of a device must be less than or equal to the minimum distance between the obstacles: $L \leq L_{ABmin}$, $\xi \leq 1$.

The maneuverability for the proposed robot is improved by reducing the distance L_{ABmin} at the third stage due to the detachment of links 1 and 5 from the surface while changing the robot’s configuration,

$$L_{ABmin} = \sum_{i=2}^4 l_i,$$

with the lifting of links 1 and 5 at angles $\theta_{21} = \theta_{45} = \pi/2$. This reduces the operating areas of the links (see Fig. 4) and allows the robot to avoid obstacles under their more dense location on the plane; hence, here $\xi > 1$. In Fig. 4, the following designations are used:  is the area outside the links of the robot,  the operating area of link 1 for $\theta_{21} = 0$,

 the operating areas of links 1 and 2 for $\theta_{21} = \pi/2$,  is the area of the possible location of obstacles within the dimensions of the robot, A is the trajectory of point O_1 for $\theta_{21} = 0$, B is the trajectory of points O_1 and O_2 for $\theta_{21} = \pi/2$, C is the trajectory of the point O_1 in the case where the robot moves forward, I is the position of the links at the beginning of the third stage and the completion of the first stage, II is the position of the links at the instant of the completion of the third stage and the beginning of the first stage, and III is the position of the links at the instant of the completion of the first stage and the beginning of the third stage.

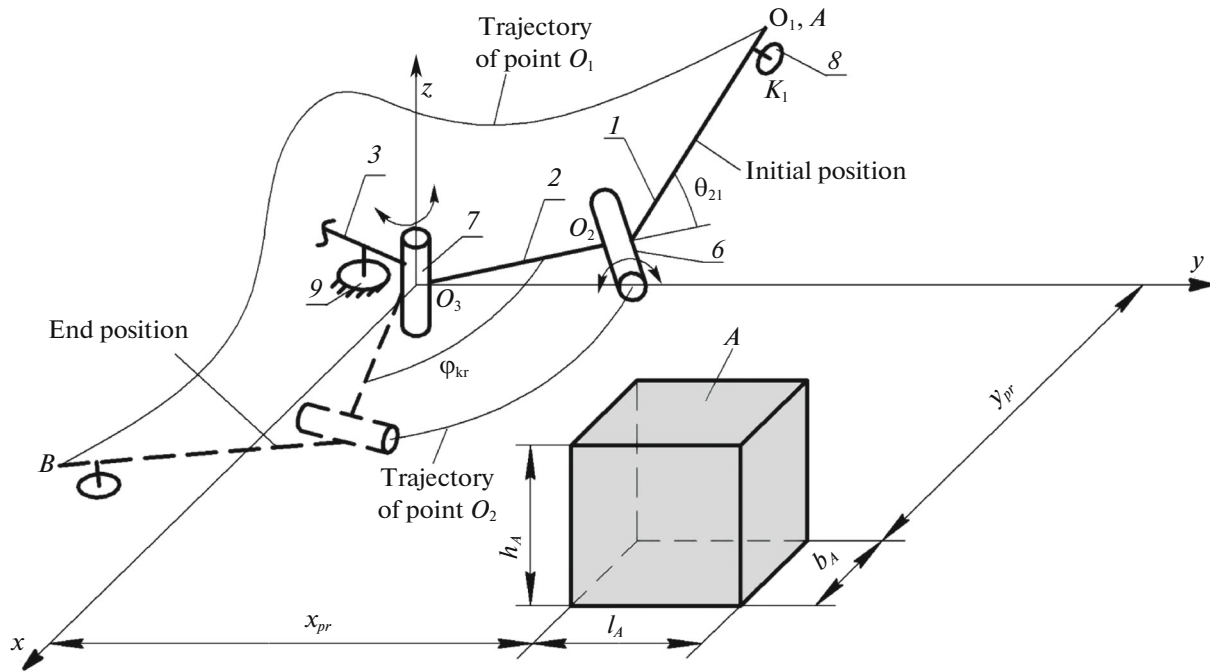

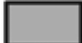


Fig. 5. Diagram of overcoming an obstacle by robot in spatial change of configuration of links.

In the first case, the robot can avoid obstacles that are outside the operating areas of the links . In the second case, the passage between the obstacles located within the operating areas of the end links is possible, except for zones bounded by links 1 and 2 (5 and 4) at the instant of the completion of the first stage (III) and curves B , i.e., the trajectories of points O_1 (O_6) during this stage: the area . The angle φ_{kr} is a certain critical angle determined by the design parameters of the robot; this angle is close to π (and in the limiting case reaches it), and with it the robot can move across the plane with obstacles.

At the third stage, links 1 and 2 (4 and 5) with link 3 fixed on the surface represent a two-dimensional spatial manipulator; they overcome an obstacle along a certain spatial trajectory from the initial point A to the end point B (see Fig. 5). Here, the form of this trajectory can vary; it depends upon the combination of the operation of drives 6 and 7 (sequential or parallel). In this paper, we consider the stepwise operation of drives 6 and 7: first the lifting of link 1 relative to link 2 by drive 6, then their joint rotation about the central link by drive 7, and then the lowering of link 1 until it interacts with the surface by drive 6. This is conditioned by the interest in investigating the influence of the drives' moments generated in the vertical planes and a horizontal plane, on the robot motion. The distances between point O_3 and an obstacle along the Ox - and Oy -axes are x_{pr} and y_{pr} .

At the first stage, the passage between obstacles can be implemented in two ways: without the interaction of the links of the robot with the obstacles (the contactless way) and with their interaction (the contact way). Assume that the location of the obstacles on the surface and their sizes are such that the links of the robot are not in contact with the obstacles. Figure 6 illustrates the contactless method of overcoming one or two small obstacles located in such a way that the displacement (in the positive direction) of the axis of motion, during the slippage of the central link, exceeds the distance at which the lateral links are pushed back (I–III correspond to the designations used in Fig. 4). In this case, the robot moves along the axis of motion without rotation about it (the vector \vec{v}_{C_3} coincides with the axis of motion; $\dot{\varphi}_3 = 0$).

2.3. Constructing the Mathematical Model

In the robot motion across a horizontal rough plane, the robot is acted upon by the following forces and moments: gravity $m_i g$ ($i = 1, \dots, 5$), normal reactions N_j ($j = 1, \dots, 4$ is the number of the support), the friction forces F_j ($j = 1, \dots, 4$), and the control moments M_{32} and M_{34} , as well as M_{21} and M_{45} . The

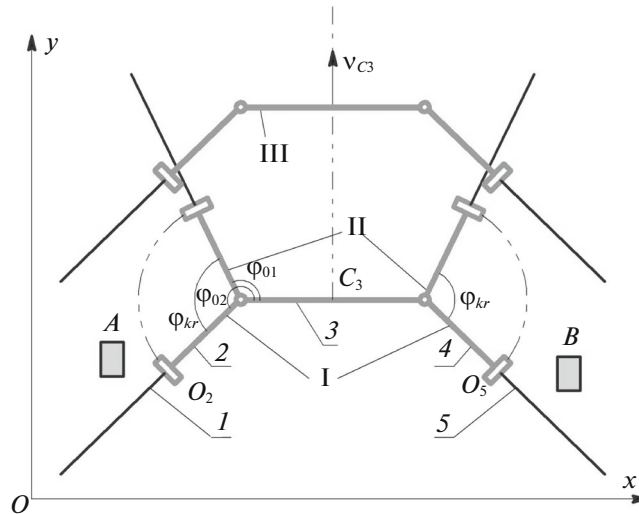


Fig. 6. Contactless way of overcoming obstacles *A* and *B*.

movement is carried out due to the friction forces F_j , which are controlled by the moments M_{32} and M_{34} , together with M_{21} and M_{45} .

In order to determine the normal reactions N_j and the friction forces F_j , we assume that they are concentrated at points K_j of the contact of the robot with the surface; here, the friction forces are described by the model of Coulomb dry friction [33]

$$F_j = \begin{cases} -f_j N_j \operatorname{sgn}(v_{K_j}) & \text{if } v_{K_j} \neq 0; \\ -F_{0j} & \text{if } v_{K_j} = 0, \quad |F_{0j}| \leq f_j N_j; \\ -f_j N_j \operatorname{sgn}(F_{0j}) & \text{if } v_{K_j} = 0, \quad |F_{0j}| > f_j N_j, \end{cases} \quad (2.1)$$

where F_{0j} is the static-friction force at point K_j , N_j is the normal reaction at point K_j , f_j is the coefficient of sliding friction, and v_{K_j} is the absolute velocity of the support at point K_j .

The projections of the friction forces on the coordinate axes are determined as follows:

$$F_{jx} = F_j \cos \alpha_j, \quad F_{jy} = F_j \sin \alpha_j,$$

where α_j is the angle between the vector of the friction force and the Ox -axis.

At points K_1 and K_4 , at all stages of the motion, the friction coefficient $f_{j=1,4} = f_{\min}$. The friction coefficient of the supports at points K_2 and K_3 is a controlled value. In the case where link 3 rests on support elements *10*, the friction coefficient $f_{j=2,3} = f_{\min}$, whereas if they are replaced by contact elements *11*, the friction coefficient $f_{j=2,3} = f_{\max} \gg f_{\min}$. It is assumed that f_{\max} is such that one eliminates the possibility of link 3 sliding. The diagram of the dependence of the friction coefficients from the stages of motion is presented in Fig. 7, where t_1 – t_4 are instants of switching between the stages.

Consider a stepwise robot motion across the plane with allowance for the generalized coordinates introduced previously; each stage of this motion is characterized by constraints imposed on the system and differential equations that describe the motion in a stage. In order to derive the equations of motion at each stage, the Lagrange equations of the second kind are used [26–28, 32]. The formulas by which one determines the normal reactions in the supports and the static-friction forces are obtained using the D'Alembert principle [26–28, 32].

We assume that the system in the initial position is at rest on four supports and the robot is acted upon by the forces of gravity, the friction forces, and the normal reactions; here, $x_{C_3} = x_{C_3}^{(0)}$ and $y_{C_3} = y_{C_3}^{(0)}$, link 3 is located at the angle $\varphi_3 = \varphi_3^{(0)}$ about the Ox -axis, links 2 and 4 are located at angles $\varphi_{32} = \varphi_{43} = \varphi_{01}$ relative to link 3, and links 1 and 5 make the angles $\theta_{21} = \theta_{54} = 0$ with links 2 and 4. Here and in the subsequent discussion, the upper index in brackets indicates the number of the state and 0 specifies the initial position. The contact of link 3 with the surface is made by supporting elements *10*.

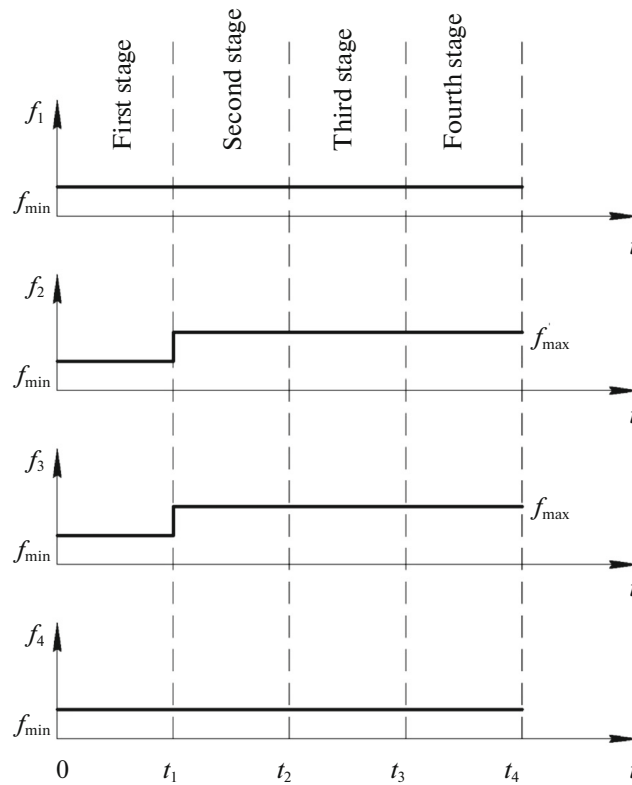


Fig. 7. Diagram of friction coefficients in supports.

Assume that at all stages of the considered mode of motion, the following conditions are fulfilled:

$$N_1 = N_4, N_2 = N_3, F_1 = F_4, F_2 = F_3.$$

If all four supports are at the surface, we consider that

$$N_1 = N_2 = N_3 = N_4.$$

Then for the normal reactions in the initial position (Fig. 8a) we have

$$N_1 = N_2 = N_3 = N_4 = \frac{1}{4} \sum_{i=1}^5 m_i g; \quad (2.2)$$

in this case, the friction forces

$$F_1 + F_2 + F_3 + F_4 = 0.$$

The first stage (moving the system forward) is characterized by the displacement of all the links of the robot in a horizontal plane under the action of moments $M_{32} = -M_{23}$ and $M_{34} = -M_{43}$; links 2 and 4 are synchronously rotated in opposite directions (together with links 1 and 5) relative to link 3, which slides forward along the axis of motion, whereas the lateral links slide back; in this event, $\theta_{21} = \theta_{54} = 0$. The motion of the system depends on four generalized coordinates: x_{C1} , y_{C1} , φ_2 , and φ_4 . The corresponding motion equations can be written as follows:

$$a_{11}^{(1)} \ddot{x}_{C1} + a_{14}^{(1)} \ddot{\varphi}_2 + a_{15}^{(1)} \ddot{\varphi}_4 + b_{14}^{(1)} \dot{\varphi}_2^2 + b_{15}^{(1)} \dot{\varphi}_4^2 = (l_1 + l_2) \sum_{j=2}^4 F_j \sin(\alpha_j - \varphi_2)/2 - M_{32},$$

$$a_{22}^{(1)} \ddot{y}_{C1} + a_{24}^{(1)} \ddot{\varphi}_2 + a_{25}^{(1)} \ddot{\varphi}_4 + b_{24}^{(1)} \dot{\varphi}_2^2 + b_{25}^{(1)} \dot{\varphi}_4^2 = M_{34} - M_{32} + l_3 \sum_{j=3,4} F_j \sin(\varphi_3 - \alpha_j),$$

$$a_{41}^{(1)}\ddot{x}_{C1} + a_{42}^{(1)}\ddot{y}_{C1} + a_{44}^{(1)}\ddot{\varphi}_2 + a_{45}^{(1)}\ddot{\varphi}_4 + b_{45}^{(1)}\dot{\varphi}_4^2 = M_{34} + F_4(l_4 + l_5)\sin(\varphi_4 - \alpha_4),$$

$$a_{51}^{(1)}\ddot{x}_{C1} + a_{52}^{(1)}\ddot{y}_{C1} + a_{54}^{(1)}\ddot{\varphi}_2 + a_{55}^{(1)}\ddot{\varphi}_4 + b_{54}^{(1)}\dot{\varphi}_2^2 = \sum_{j=1}^4 F_j \sin \alpha_j,$$

where $a_{kp}^{(d)}$ and $b_{kp}^{(d)}$ ($k = \overline{1,6}$, $p = \overline{1,6}$, and $d = \overline{1,4}$) are coefficients which represent the set of the geometric and mass characteristics of the robot's links; F_j is determined by formula (2.1) taking into account (2.2), during which at this stage the friction coefficient $f_{j=2,3} = f_{\min}$. At this stage, the formulas of the normal reactions coincide with the determination of the same values in the initial position. The stage ends when angles φ_{32} and φ_{34} attain the value of $\varphi_{32}^{(1)} = \varphi_{43}^{(1)} = \varphi_{02}$; in this case, $x_{C3} = x_{C3}^{(1)}$, $y_{C3} = y_{C3}^{(1)}$, and $\varphi_3 = \varphi_3^{(1)}$. All subsequent steps are carried out with the stationary link 3; this is achieved by the interaction with the surface of support elements II ($f_{j=2,3} = f_{\max} \gg f_{\min}$).

At the second stage (the lifting of the end links), the lifting of links 1 and 5 and the detachment of their supports from the surface are carried out due to the action of moments M_{21} and M_{45} , which are equal in magnitude and opposite in direction. In the process of this stage, link 3 remains stationary: $x_{C3} = x_{C3}^{(1)}$, $y_{C3} = y_{C3}^{(1)}$, and $\varphi_3 = \varphi_3^{(1)}$, during which $\varphi_{32} = \varphi_{43} = \varphi_{02}$. The movement of links 1 and 5 is described by two equations for the generalized θ_1 and θ_5 coordinates:

$$a_{33}^{(2)}\ddot{\theta}_1 = -M_{21} + m_1gl_1 \cos \theta_1/2, \quad a_{66}^{(2)}\ddot{\theta}_5 = M_{45} - m_5gl_5 \cos \theta_5/2.$$

The condition of the completion of this stage is $\theta_{21}^{(2)} = \theta_{54}^{(2)} = \theta_0$. The normal reactions and the projections of the friction forces are determined by the formulas (see Fig. 8b)

$$N_2 = N_3 = \frac{1}{2} \left(\sum_{i=1}^5 m_i g + \sum_{i=1,5} m_i \ddot{z}_{Ci} \right),$$

$$F_{2x} = F_{3x} = -\frac{1}{2} \sum_{i=1,2,4,5} m_i \ddot{x}_{Ci}, \quad F_{2y} = F_{3y} = -\frac{1}{2} \sum_{i=1,2,4,5} m_i \ddot{y}_{Ci}.$$

At the stages of the lifting and the lowering of links 1 and 5, of greater importance is the solution of the stability problem for the plant on two supports 9 of the central link. The minimum required length l_p of support 9 is determined using the ZMP (zero-moment point) method, according to which the zero-moment point must lie within the support surface 9, and this allows one to avoid the device overturning [34, 35]. Consider the location of links 2 and 3, as well as 3 and 4 at angles $\varphi_{32} = \varphi_{43} = \pi/2$ and $\theta_{21} = \theta_{54}$ such that the maximum overturning moment arises. Figure 9 shows the forces applied to links 1–3, namely, the gravitational forces m_1g , m_2g , and m_3g and the inertial force Φ_{lu} , which depends on the rotation of link 1 in a vertical plane and has the normal Φ_{lun} and tangential Φ_{lut} components. The minimum required length of support 9 is determined by the formula

$$l_p = \frac{gl_2(2m_1 + m_2) + m_1gl_1 \cos \theta_{21} + m_1l_1z_p(\dot{\theta}_{21}^2 \cos \theta_{21} + \ddot{\theta}_{21} \sin \theta_{21}) + m_1l_1l_2Q - 2m_1l_1^2\ddot{\theta}_{21}/3}{2g(m_1 + m_2) + m_3g + m_1l_1Q},$$

where $Q = \ddot{\theta}_{21} \cos \theta_{21} - \dot{\theta}_{21}^2 \sin \theta_{21}$.

At the third stage (changing the configuration of the links in a horizontal plane), link 3 remains stationary: $x_{C3} = x_{C3}^{(1)}$, $y_{C3} = y_{C3}^{(1)}$, and $\varphi_3 = \varphi_3^{(1)}$. Links 1 and 2, along with links 4 and 5 rotate due to the action of moments M_{32} and M_{34} , which are equal in magnitude and opposite in direction, until the condition $\varphi_{32}^{(3)} = \varphi_{43}^{(3)} = \varphi_{01}$ (the condition of the stage's completion) is fulfilled; here, $\theta_{21} = \theta_{54} = \theta_0$. The robot motion is described by two equations for the generalized φ_2 and φ_4 coordinates:

$$a_{44}^{(3)}\ddot{\varphi}_2 = -M_{32}, \quad a_{55}^{(3)}\ddot{\varphi}_4 = M_{34}.$$

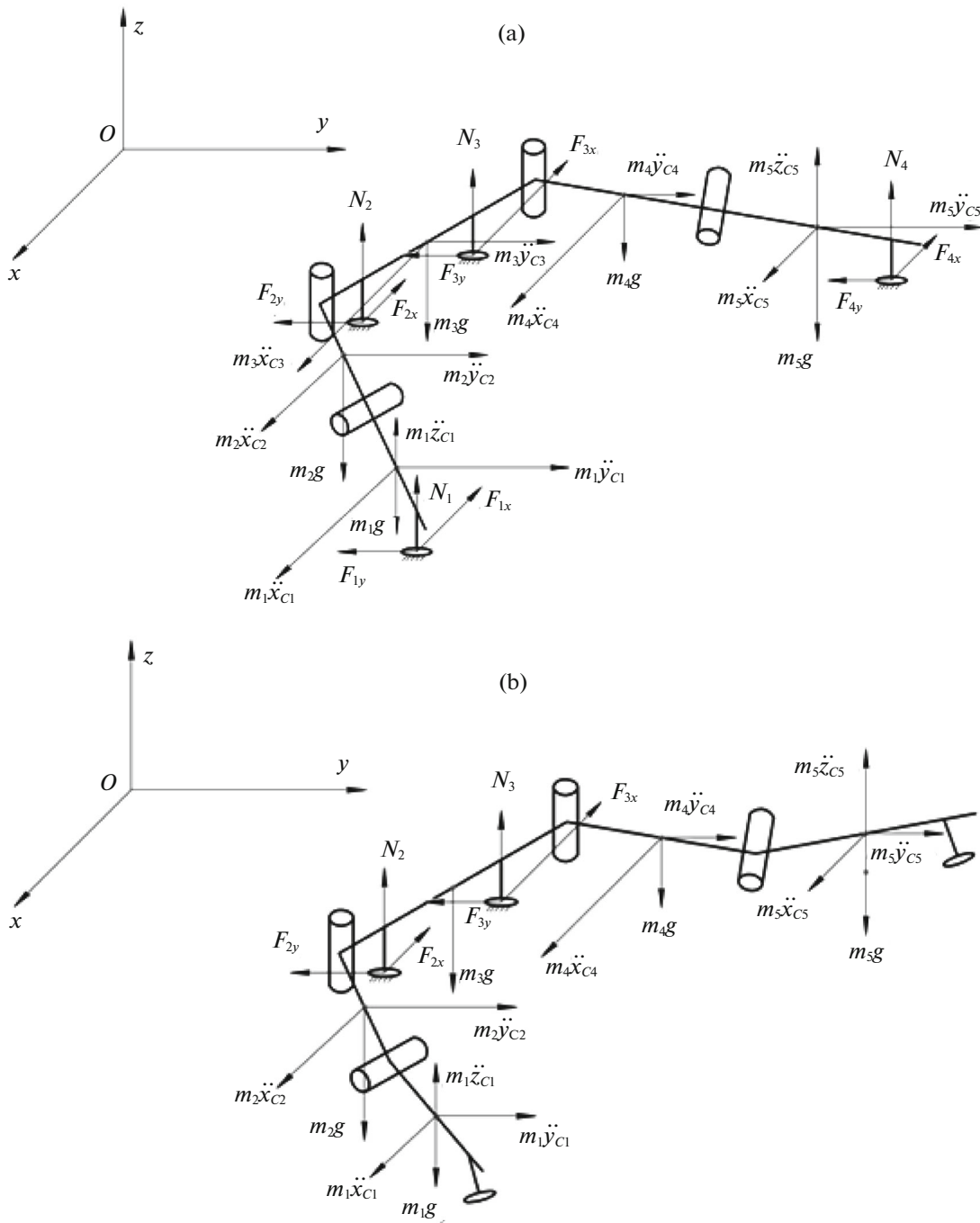


Fig. 8. Diagrams of determining normal reactions and friction forces: (a) four contact points and (b) two contact points.

The normal reactions are determined as follows (see Fig. 8b):

$$N_2 = N_3 = \frac{1}{2} \sum_{i=1}^5 m_i g.$$

The friction forces are determined by the formulas of the second stage.

At the fourth stage (the lowering of the end links), link 3 lies stationary on the surface: $x_{C3} = x_{C3}^{(1)}$, $y_{C3} = y_{C3}^{(1)}$, and $\varphi_3 = \varphi_3^{(1)}$. The stage consists in the rotation of links 1 and 5 relative to links 2 and 4 in the

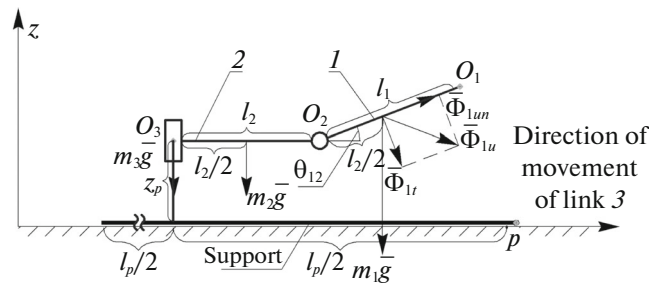


Fig. 9. Diagram of forces applied to links 1–3 for determining length of support 9 by ZMP method.

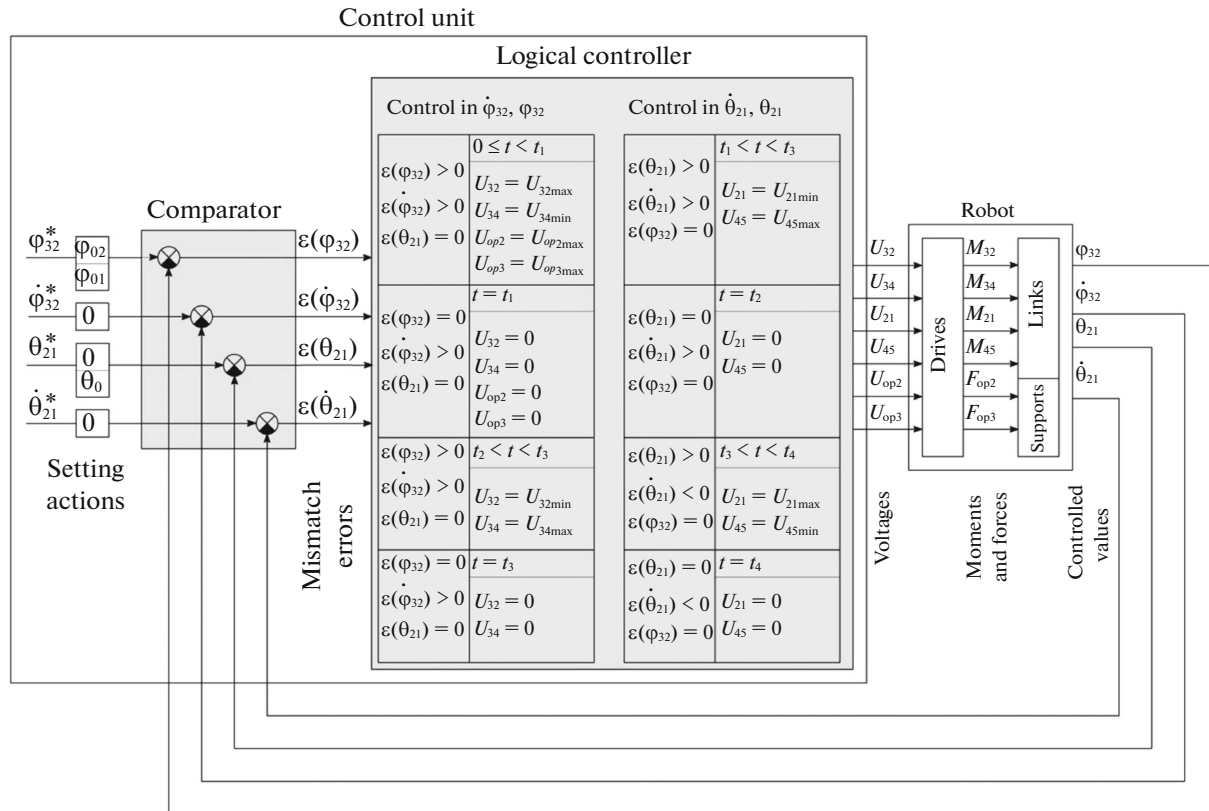


Fig. 10. Functional diagram of robot's control system.

vertical planes due to the action of moments M_{21} and M_{45} , which are equal in magnitude and opposite in direction, until the equality for the relative angles $\theta_{21}^{(4)} = \theta_{54}^{(4)} = 0$ is fulfilled. Here, the contact points K_1 and K_4 interact with the surface and the normal reactions have the same values as at the first stage: $N_1^{(4)} = N_4^{(4)} = N_1^{(1)} = N_4^{(1)}$. The directions of moments M_{21} and M_{45} are opposite to the specified directions for the second stage, while the equations correspond to the second stage; in this case, $\varphi_{32} = \varphi_{43} = \varphi_{01}$. The normal reactions and the friction forces are determined in the same way as in the second stage. At the instant the stage ends, the robot is found in the initial position; link 3 comes into contacts with the surface by support elements 10.

3. CONTROL SYSTEM

The robot moves due to the control system (see Fig. 10). Assume that the system generates piecewise constant voltages $U_{32}, U_{34}, U_{21}, U_{45}, U_{op2}$, and U_{op3} , which are applied to the drives of the robot during

certain time intervals determined by the relative angles φ_{32} , φ_{43} , θ_{21} , and θ_{54} of the rotation of the links and their angular velocities $\dot{\varphi}_{32}$, $\dot{\varphi}_{43}$, $\dot{\theta}_{21}$, and $\dot{\theta}_{54}$. In accordance with the relative angles φ_{32} , φ_{43} , θ_{21} , and θ_{54} of the rotation of the links and their angular velocities $\dot{\varphi}_{32}$, $\dot{\varphi}_{43}$, $\dot{\theta}_{21}$, and $\dot{\theta}_{54}$, one finds the instants t_1-t_4 of switching between stages of motion:

$$\begin{aligned} t_1: \varphi_{32}(t_1) &= \varphi_{43}(t_1) = \varphi_{02}, \theta_{21}(t_1) = \theta_{54}(t_1) = 0, \\ t_2: \theta_{21}(t_2) &= \theta_{54}(t_2) = \theta_0, \varphi_{32}(t_2) = \varphi_{43}(t_2) = \varphi_{02}, t_2 > t_1, \\ t_3: \varphi_{32}(t_3) &= \varphi_{43}(t_3) = \varphi_{01}, \theta_{21}(t_3) = \theta_{54}(t_3) = \theta_0, t_3 > t_2, \\ t_4: \theta_{21}(t_4) &= \theta_{54}(t_4) = 0, \varphi_{32}(t_4) = \varphi_{43}(t_4) = \varphi_{01}, t_4 > t_3; \end{aligned}$$

here, the following time intervals of the stages are formed:

$$\begin{aligned} t \in [0, t_1) \quad &\text{if} \quad \varphi_{32}, \varphi_{43} \in [\varphi_{01}, \varphi_{02}), \dot{\varphi}_{32} > 0, \dot{\varphi}_{43} < 0, \theta_{21} = \theta_{54} = 0, \\ t \in [t_1, t_2) \quad &\text{if} \quad \theta_{21}, \theta_{54} \in [0, \theta_0), \dot{\theta}_{21} > 0, \dot{\theta}_{54} < 0, \varphi_{32} = \varphi_{43} = \varphi_{02}, \\ t \in [t_2, t_3) \quad &\text{if} \quad \varphi_{32}, \varphi_{43} \in [\varphi_{01}, \varphi_{02}), \dot{\varphi}_{32} < 0, \dot{\varphi}_{43} > 0, \theta_{21} = \theta_{54} = \theta_0, \\ t \in [t_3, t_4] \quad &\text{if} \quad \theta_{21}, \theta_{54} \in [0, \theta_0), \dot{\theta}_{21} < 0, \dot{\theta}_{54} > 0, \varphi_{32} = \varphi_{43} = \varphi_{01}. \end{aligned}$$

The control system consists of the control unit, which includes the comparator and the logical controller, and the control plant, which represents the crawling robot. The input of the comparator receives setting actions, which represent the relative rotation angles of links 2 and 3, 4 and 3, 2, and 1, along with 5 and 4 (φ_{32}^* , φ_{43}^* , θ_{21}^* , and θ_{54}^*), as well as the relative angular velocities $\dot{\varphi}_{32}^*$, $\dot{\varphi}_{43}^*$, $\dot{\theta}_{21}^*$, and $\dot{\theta}_{54}^*$. The values of the setting actions are presented as follows:

$$\begin{aligned} \varphi_{32}^*, \varphi_{43}^* &= \begin{cases} \varphi_{01}, & t \in [t_2, t_4], \\ \varphi_{02}, & t \in [0, t_2); \end{cases} \quad \theta_{21}^*, \theta_{54}^* = \begin{cases} 0, & t \in [0, t_1) \cap [t_3, t_4], \\ \theta_0, & t \in [t_1, t_3); \end{cases} \\ \dot{\varphi}_{32}^* &= \begin{cases} > 0, & t \in [t_2, t_4], \\ < 0, & t \in [0, t_2); \end{cases} \quad \dot{\theta}_{21}^* = \begin{cases} < 0, & t \in [0, t_1) \cap [t_3, t_4], \\ > 0, & t \in [t_1, t_3); \end{cases} \\ \dot{\varphi}_{43}^* &= \begin{cases} < 0, & t \in [t_2, t_4], \\ > 0, & t \in [0, t_2); \end{cases} \quad \dot{\theta}_{54}^* = \begin{cases} > 0, & t \in [0, t_1) \cap [t_3, t_4], \\ < 0, & t \in [t_1, t_3). \end{cases} \end{aligned}$$

The comparator compares the setting values with the controlled values, namely, the factual values of the rotation angles φ_{32} , φ_{43} , θ_{21} , and θ_{54} of the links and their angular velocities $\dot{\varphi}_{32}$, $\dot{\varphi}_{43}$, $\dot{\theta}_{21}$, and $\dot{\theta}_{54}$. The mismatch errors between signals

$$\varepsilon(\varphi_{32}) = \varphi_{32}^* - \varphi_{32}, \quad \varepsilon(\dot{\varphi}_{32}) = \dot{\varphi}_{32}^* - \dot{\varphi}_{32},$$

$$\varepsilon(\varphi_{43}) = \varphi_{43}^* - \varphi_{43}, \quad \varepsilon(\dot{\varphi}_{43}) = \dot{\varphi}_{43}^* - \dot{\varphi}_{43},$$

$$\varepsilon(\theta_{21}) = \theta_{21}^* - \theta_{21}, \quad \varepsilon(\dot{\theta}_{21}) = \dot{\theta}_{21}^* - \dot{\theta}_{21},$$

$$\varepsilon(\theta_{54}) = \theta_{54}^* - \theta_{54}, \quad \varepsilon(\dot{\theta}_{54}) = \dot{\theta}_{54}^* - \dot{\theta}_{54}$$

arrive at the logical controller, which contains two units. One of them exerts control depending upon the mismatch errors of the angular values in a horizontal plane $\varepsilon(\varphi_{32})$, $\varepsilon(\dot{\varphi}_{32})$, $\varepsilon(\varphi_{43})$, and $\varepsilon(\dot{\varphi}_{43})$, while the second unit, exerts control in the vertical planes: $\varepsilon(\theta_{21})$, $\varepsilon(\dot{\theta}_{21})$, $\varepsilon(\theta_{54})$, and $\varepsilon(\dot{\theta}_{54})$. The controller determines the instants t_1-t_4 of switching between the stages and forms time laws for varying voltages U_{32} , U_{34} , U_{21} , U_{45} , U_{op2} , and U_{op3} at each stage. In this case, the first unit of the controller is responsible for voltages U_{32} , U_{34} , U_{op2} , and U_{op3} , whereas the second unit is responsible for voltages U_{21} and U_{45} .

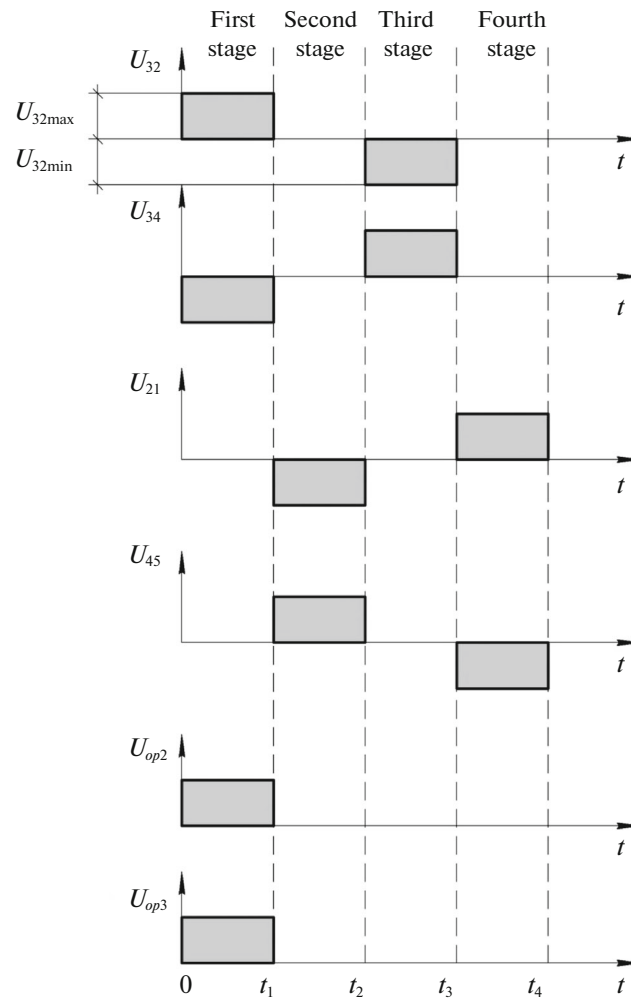


Fig. 11. Voltage diagram.

The algorithm of forming the voltages we present as follows (the diagram is shown in Fig. 11):

$$U_{32} = \begin{cases} U_{32\max}, & 0 \leq t < t_1, \\ U_{32\min}, & t_2 \leq t < t_3, \\ 0, & (t_1 \leq t < t_2) \cap (t_3 \leq t \leq t_4); \end{cases} \quad U_{34} = \begin{cases} U_{34\min}, & 0 \leq t < t_1, \\ U_{34\max}, & t_2 \leq t < t_3, \\ 0, & (t_1 \leq t < t_2) \cap (t_3 \leq t \leq t_4); \end{cases}$$

$$U_{21} = \begin{cases} U_{21\max}, & t_3 \leq t \leq t_4, \\ U_{21\min}, & t_1 \leq t < t_2, \\ 0, & (0 \leq t < t_1) \cap (t_2 \leq t < t_3); \end{cases} \quad U_{45} = \begin{cases} U_{45\min}, & t_3 \leq t \leq t_4, \\ U_{45\max}, & t_1 \leq t < t_2, \\ 0, & (0 \leq t < t_1) \cap (t_2 \leq t < t_3); \end{cases}$$

$$U_{op2} = \begin{cases} U_{op2\max}, & 0 \leq t < t_1, \\ 0, & (t_1 \leq t \leq t_4); \end{cases} \quad U_{op3} = \begin{cases} U_{op3\max}, & 0 \leq t < t_1, \\ 0, & (t_1 \leq t \leq t_4). \end{cases}$$

The voltages represent piecewise constant functions of time; their level is chosen from specific constructive considerations and can be optimized depending upon the chosen criterion (the maximum average motion velocity, the minimum power consumption, etc.). The signals in question arrive at the drives of the robot and we form the moments and the forces there:

$$M_{32} = k_{32}i_{32}, \quad M_{34} = k_{34}i_{34},$$

$$M_{21} = k_{21}i_{21}, \quad M_{45} = k_{45}i_{45},$$

$$F_{op2} = k_{op2}i_{op2}, \quad F_{op3} = k_{op3}i_{op3}$$

proportional to the motors' currents i_{32} , i_{34} , i_{21} , i_{45} , i_{op2} , and i_{op3} , which are determined by the equation of an electric drive [36]. The obtained moments arrive at the links of the device and provide their rotations relative to each other in the horizontal and vertical planes at the angles φ_{32} , φ_{43} , θ_{21} , and θ_{54} with the angular velocities $\dot{\varphi}_{32}$, $\dot{\varphi}_{43}$, $\dot{\theta}_{21}$, and $\dot{\theta}_{54}$, while the forces arrive at the supports of link 3 of the robot and change the coefficient of friction f_{\min}/f_{\max} between them and the surface.

4. SIMULATION OF THE ROBOT MOTION

The robot motion across the plane is simulated numerically by a specifically developed algorithm, which provides switching between the stages of the motion when the links' rotation angles take their end values. Here, a counter n that takes values from one to four and corresponds to the number of a stage is used. The simulated robot has the following parameters: the lengths of the links $l_1 = l_5 = 108$ mm, $l_2 = l_4 = 0$, and $l_3 = 100$ mm; the masses of the links $m_1 = m_5 = 45$ g, $m_2 = m_4 = 0$, and $m_3 = 70$ g (i.e., it is assumed that the lengths and the masses of links 2 and 4 are negligibly small in comparison to the lengths and the masses of the other links); the amplitudes of the moments generated by drives $M_{32} = M_{34} = 0.002$ N m and $M_{21} = M_{45} = 0.02$ N m; and the height of the supports $z_{C3} = 0$.

4.1. Testing

In order to check the adequacy of the developed mathematical model, it was tested by constructing and analyzing the graphs of the time dependences of the generalized coordinates and their derivatives for three variants of the attained angles: (1) $\varphi_{01} = \pi/2$, $\varphi_{02} = -\pi/2$, and $\theta_0 = \pi/4$; (2) $\varphi_{01} = \pi/2$, $\varphi_{02} = 0$, and $\theta_0 = \pi/2$; and (3) $\varphi_{01} = 0$, $\varphi_{02} = -\pi/2$, and $\theta_0 = \pi/2$. The curves in Figs. 12–14 correspond to the following values of the angles: 1, 3, and 5 fit $\varphi_{01} = \pi/2$, $\varphi_{02} = -\pi/2$, and $\theta_0 = \pi/4$; 1', 3', and 5' fit $\varphi_{01} = \pi/2$, $\varphi_{02} = 0$, and $\theta_0 = \pi/2$; and 1'', 3'', and 5'' fit $\varphi_{01} = 0$, $\varphi_{02} = -\pi/2$, and $\theta_0 = \pi/2$.

Figure 12 presents the graphs of the time dependences of the projections of the coordinates for the centers of mass of the links along the Ox -, Oy -, and Oz -axes. Figure 12a shows that along the Ox -axis the central link 3 remains stationary and links 1 and 5 move symmetrically about the origin. Here, the centers of mass of links 1 and 5 move along the Ox -axis at the first stage independently of the values of angles φ_{01} , φ_{02} , and θ_0 , while at the third stage, they move only in the case where $\theta_0 \neq \pi/2$ (graphs 1 and 5), as the rotation of links located normally to the surface about a vertical axis does not cause a change of the coordinates of their centers of mass. At the second stage, the lateral links do not move along the Ox -axis only when $\varphi_{02} = -\pi/2$ (graphs 1 and 5, together with 1'' and 5''), while at the fourth stage, when $\varphi_{01} = \pi/2$ (graphs 1 and 5, along with 1' and 5'), i.e., in the case where the links are located in a horizontal plane along the axis of motion. According to Fig. 12b, link 3 moves in the positive direction of the Oy -axis only at the first stage. In parallel, the end links of the robot move in the opposite direction; here, the distance covered by them is less than the distance covered by the central link. At all other stages, link 3 remains stationary and links 1 and 5 move forward along the Oy -axis: at the second stage, due to their lifting; at the third stage, due to the rotation relative to link 3; and at the fourth stage, due to being lowered to the surface. The central link covers the largest distance along the Oy -axis at the largest range of the rotation angle of the lateral links in a horizontal plane $\varphi_{01} - \varphi_{02} = \pi$ (graph 3); in the two other cases, $\varphi_{01} - \varphi_{02} = \pi/2$ and the distances covered by the central link are identical.

The graphs of the time dependences along the Oz -axis (Fig. 12c) demonstrate that link 3 never comes off the surface, during which links 1 and 5, in the process of the first stage, are located on the surface, move up at the second stage and attain angle θ_0 to the time of the completion of the stage, remain at a fixed height during the third stage, and move down during the fourth stage until the angles of their inclination to the horizon become 0 rad.

Also note that under the equal ranges of the change in the rotation angle of the lateral links in a horizontal plane, the durations of the first stages are almost identical; this stage is completed slightly faster when $\varphi_{01} = 0$ and $\varphi_{02} = -\pi/2$. The time ranges of the other three stages in both cases are identical. When $\varphi_{01} - \varphi_{02} = \pi$, the first and third stages continue for a longer time, whereas the second and fourth stages continue for a shorter time, because $\theta_0 = \pi/4$ and not $\theta_0 = \pi/2$.

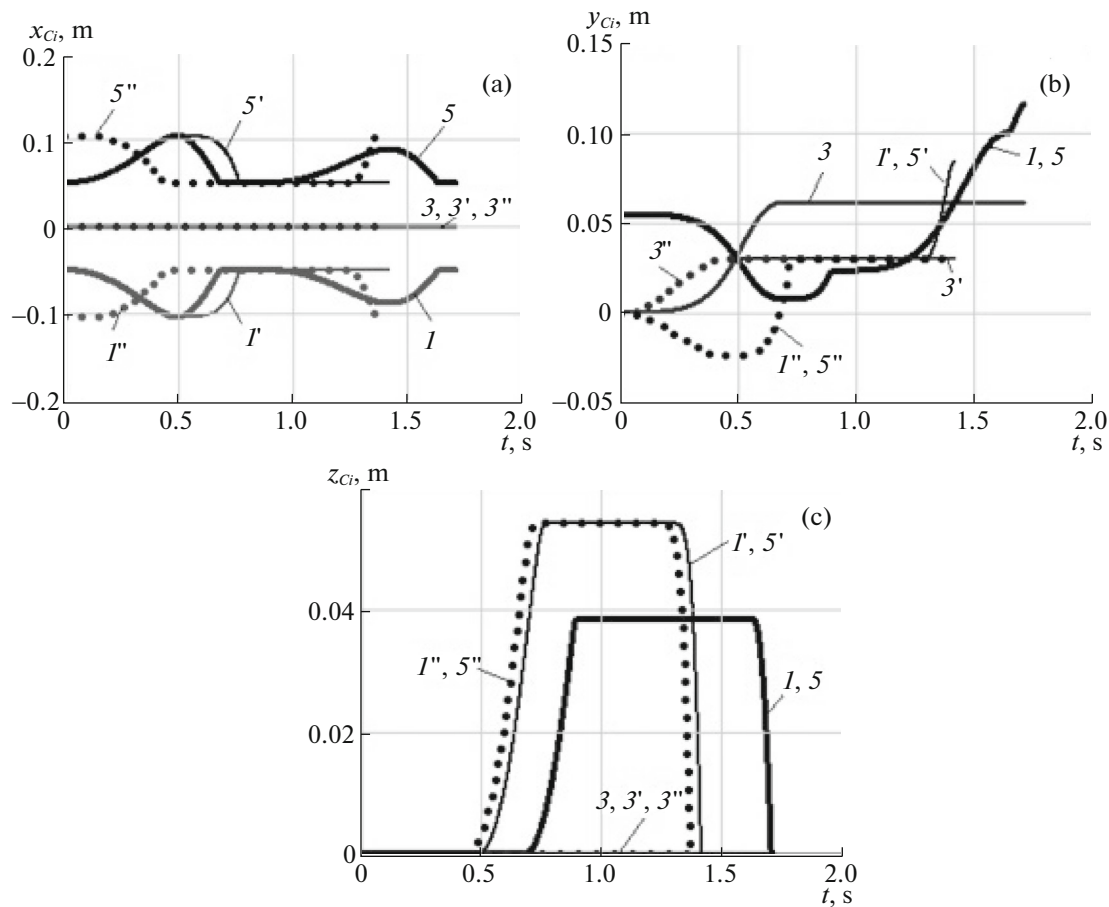


Fig. 12. Graphs of time dependences of projections of coordinates for centers of mass of links: (a) $x_{Ci}(t)$, (b) $y_{Ci}(t)$, and (c) $z_{Ci}(t)$.

The graphs in Fig. 13 confirm the correctness of the mathematical model in relation to the rotation angles of the links: the central link does not rotate in the horizontal and vertical planes during the entire movement, while the rotation angles of links I and 5 change with time in inverse manner relative to 0 rad; i.e., the values of their rotation angles at each instant are equal in magnitude and opposite in direction. The values attained by the angles at each stage also illustrate the justice of the performed simulation, because they correspond to the values specified in the model.

Figure 14 shows that the angular velocities of the rotation of links I and 5 in a horizontal plane and vertical planes are equal in magnitude and opposite in direction, while for link 3 , these velocities are zero. Here, the lateral links rotate in the horizontal plane during the first and third stages and in the vertical planes, during the second and fourth stages. The angular velocities at the beginning of the stages always have zero values, increase in magnitude by proportional or curvilinear laws, attain the largest values by the instants of the completion of the stages, and are sharply zeroed.

According to Fig. 15, the relative rotation angles of the lateral links in every simulated case are changed by the same laws (I and 5 for $\varphi_{01} = \pi/2$, $\varphi_{02} = -\pi/2$, and $\theta_0 = \pi/4$; I' and $5'$ for $\varphi_{01} = \pi/2$, $\varphi_{02} = 0$, and $\theta_0 = \pi/2$; and I'' and $5''$ for $\varphi_{01} = 0$, $\varphi_{02} = -\pi/2$, and $\theta_0 = \pi/2$). In a horizontal plane, the angles at the first stage decrease according to certain curves, the convexities of which are directed upwards from the initial values equal to φ_{01} , and take values of φ_{02} by the time of the completion of the first stage; they remain constant at the second stage; they increase at the third stage by the curves, which represent arcs of the circles, from φ_{02} to φ_{01} ; and they also remain fixed at the fourth stage. In the vertical planes, the angles at the first and third stages are equal to 0 rad and θ_0 , respectively; during the second stage, they gradually increase from 0 to θ_0 ; and during the fourth stage, conversely, they gradually decrease from θ_0 to 0 .

Note that the time of the first and third stages is significantly longer than the time of the second and fourth stages. In addition, all the presented graphs demonstrate that the values of, first, the coordinates'

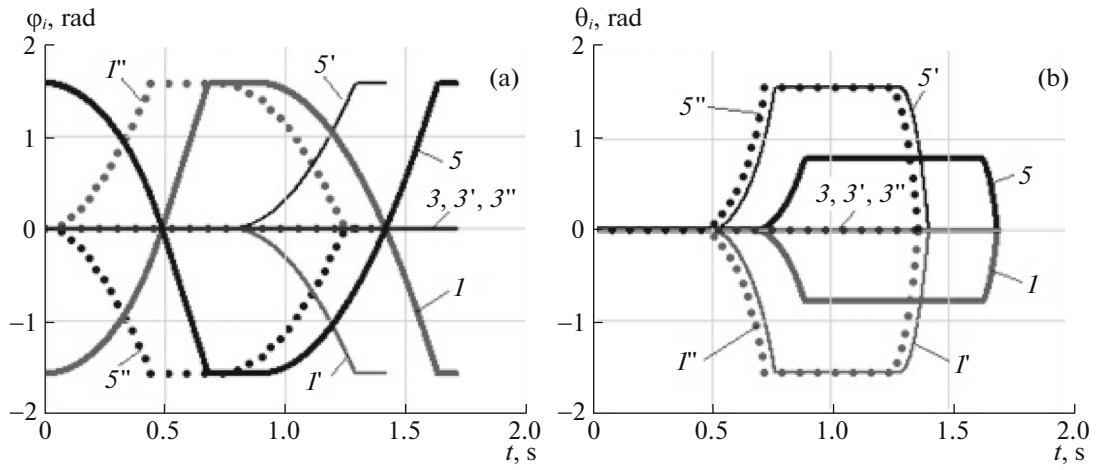


Fig. 13. Graphs of time dependences of rotation angles of links: (a) $\phi_i(t)$ and (b) $\theta_i(t)$.

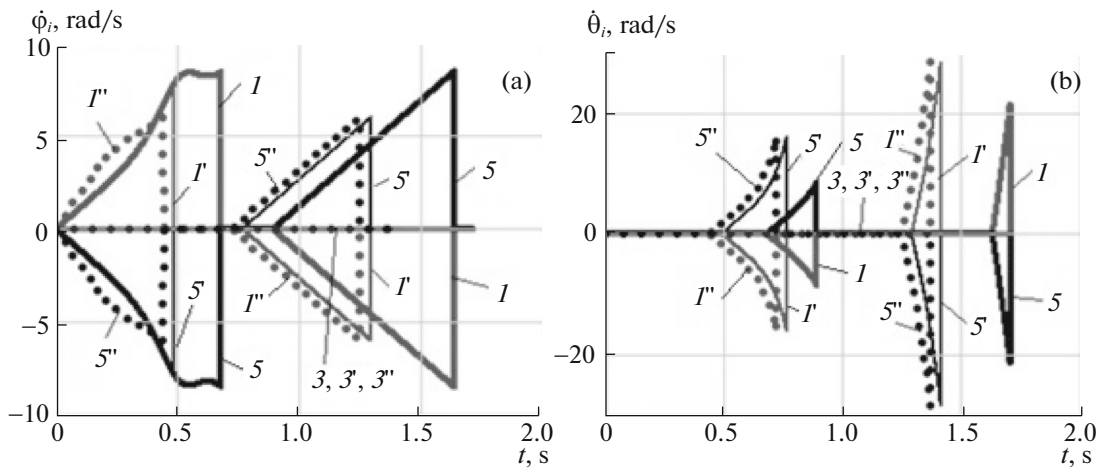


Fig. 14. Graphs of time dependences of angular velocities of links: (a) $\dot{\phi}_i(t)$ and (b) $\dot{\theta}_i(t)$.

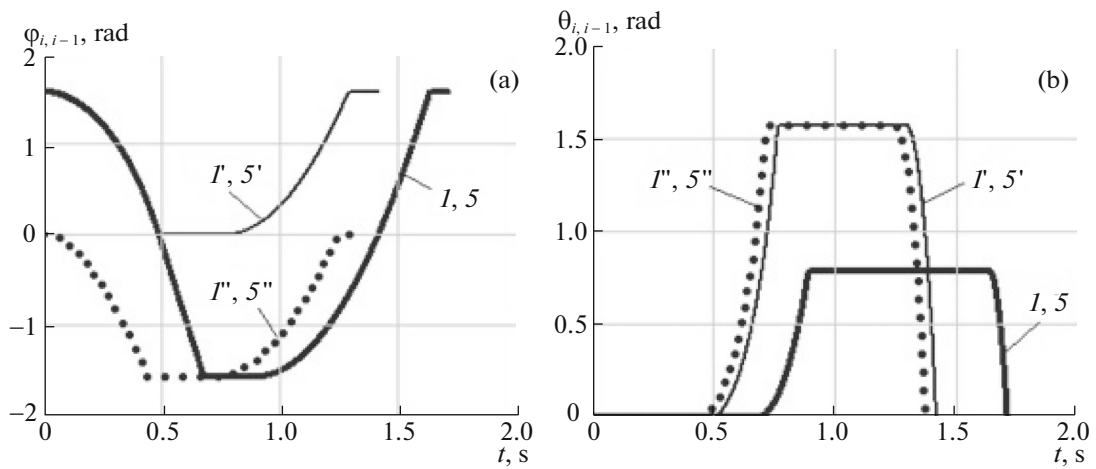


Fig. 15. Graphs of time dependences of relative rotation-angles of links: (a) $\phi_{i,i-1}(t)$ during which I, I' , and I'' fit $\varphi_{32}(t)$ and $5, 5',$ and $5''$ fit $\varphi_{43}(t)$ as well as (b) $\theta_{i,i-1}(t)$ during which $I, I',$ and I'' fit $\theta_{21}(t)$ and $5, 5',$ and $5''$ fit $\theta_{54}(t)$.

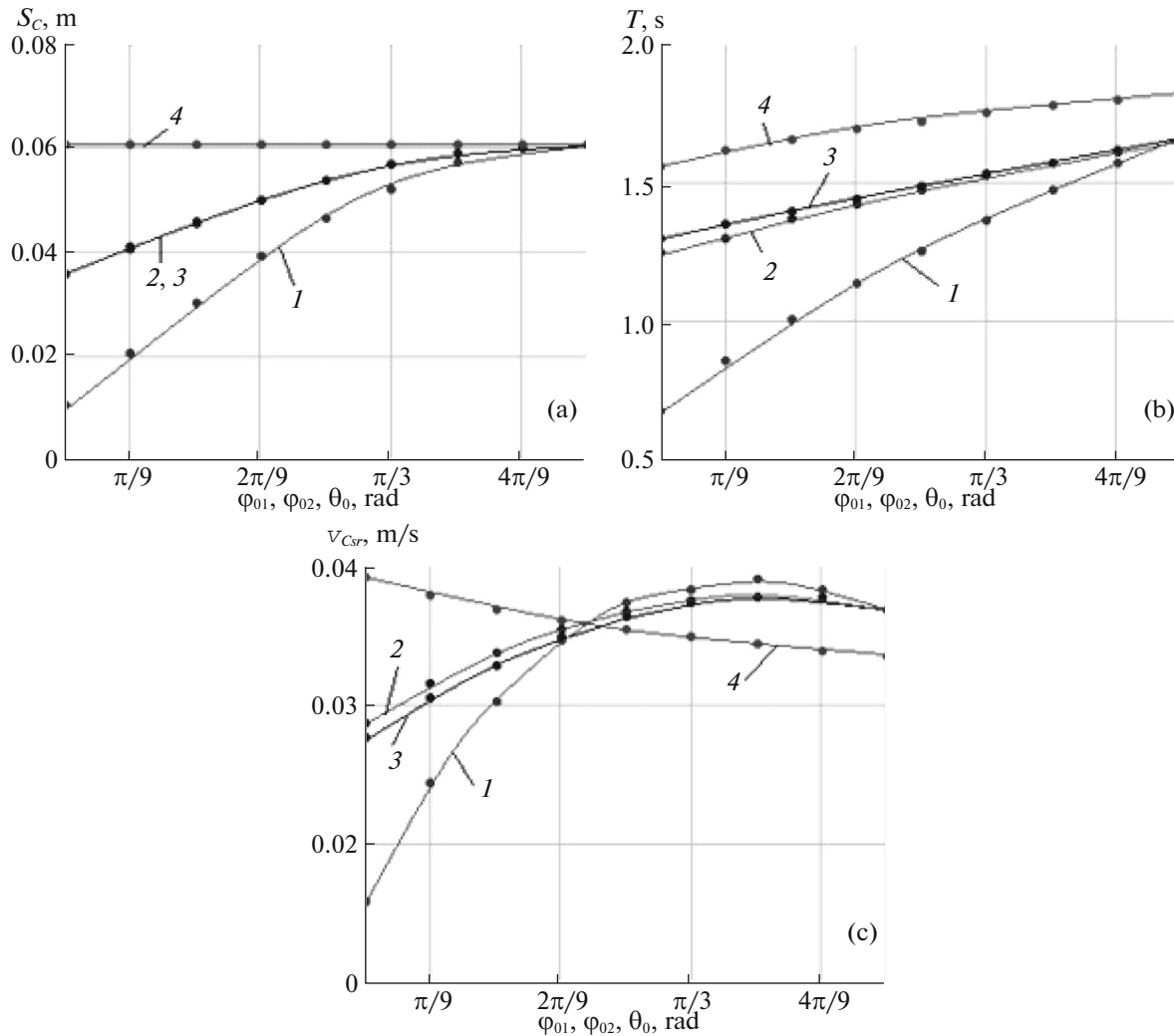


Fig. 16. Graphs of (a) distance S_C , (b) time T , and (c) average velocity v_{Csr} against amplitudes of rotation angles of links: (1) $\varphi_{01} = \varphi_{02}$ for $\theta_0 = \pi/2$, (2) φ_{01} for $\varphi_{02} = \pi/2$ and $\theta_0 = \pi/2$, (3) φ_{02} for $\varphi_{01} = \pi/2$ and $\theta_0 = \pi/2$, and (4) θ_0 for $\varphi_{01} = \varphi_{02} = \pi/2$.

projections of the centers of mass of the links, second, the angles of their rotation, and, third, the angular velocities at the initial instant of the simulation and after four stages are identical.

4.2. Investigation of the Average Velocity

Figures 16 and 17 present the results of investigating the influence of the control parameters on the average velocity of the robot motion; here, the control parameters are the largest values of the angles of the links' rotation in the horizontal φ_{01} and φ_{02} and vertical θ_0 planes, as well as of the amplitudes of the moments $M_{32\max}$, $M_{34\max}$, $M_{21\max}$, and $M_{45\max}$ of the drives in the form of dependences of the distance covered during the four stages by the center of mass of link 3, the time spent on this, and the average velocity of the varied values. The average velocity is determined by the formula $v_{Csr} = S_C/T$, where S_C is the distance covered by the center of mass of the robot along its transverse axis for one cycle (four stages) and T is the time of one cycle.

The character of changing the average velocity of the robot from the values of φ_{01} , φ_{02} , and θ_0 is demonstrated in Fig. 16. The graphs show that with values of angles φ_{01} and φ_{02} increasing from 0 to $7\pi/9$, the average velocity of the robot increases and then decreases. In this case, at angles $0 \leq \varphi_{01}, \varphi_{02} \leq 4\pi/9$ the

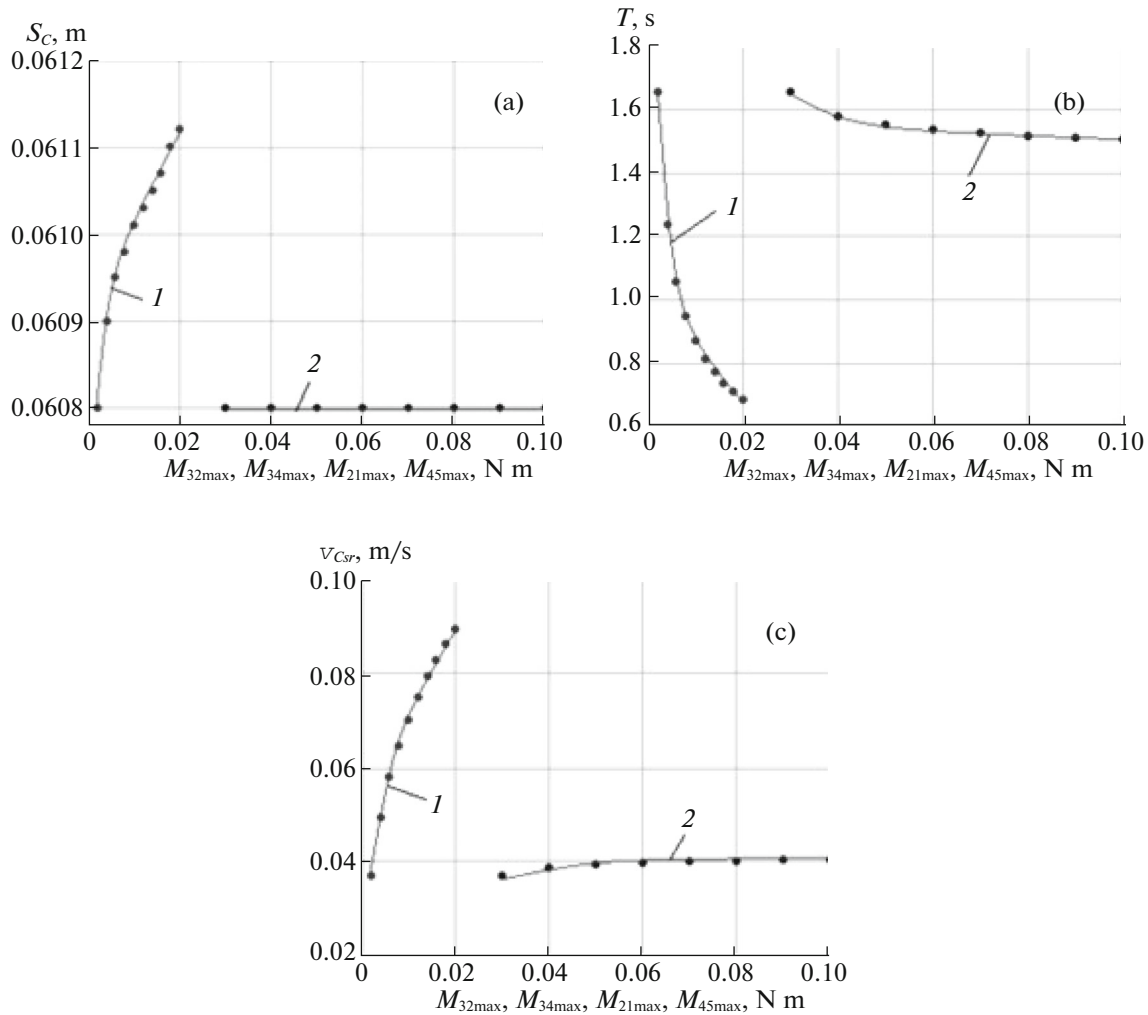


Fig. 17. Graphs of (a) distance S_C , (b) time T , and (c) average velocity v_{Csr} against control moments: (1) M_{32max} and M_{34max} as well as (2) M_{21max} and M_{45max} .

dependence is proportional and at $4\pi/9 < \varphi_{01}, \varphi_{02} \leq \pi/2$ the graph is curvilinear, during which its convexity is directed upwards; starting from $\varphi_0 = 4\pi/9$, the increase in the average velocity with increasing φ_{01} and φ_{02} is insignificant. Besides, it is seen that in the cases where φ_{01} or φ_{02} is $\pi/2$, the average velocity varies according to almost the same law, depending upon the varied parameter φ_{02} (φ_{01}). If $\varphi_{01} = \varphi_{02}$, then in the area of the proportional increase of the average velocity, this curve is positioned significantly below the two curves considered earlier; for $\varphi_{01} = \varphi_{02} = 4\pi/9$, all three curves take almost the identical values; and on the interval $4\pi/9 < \varphi_{01}, \varphi_{02} \leq \pi/2$, the third curve is positioned slightly higher. Hence, it can be concluded that in order to increase the average velocity of the robot motion, it is necessary that one of the two angles, φ_{01} or φ_{02} , takes the value $\pi/2$ and the second angle does not exceed $4\pi/9$, or one or two angles take the value $7\pi/9$.

For $\varphi_{01} = \pi/2$ and for $\varphi_{02} = \pi/2$, the distances covered by the center of mass of the central link in the four stages are identical, whereas the time spent on the passage of the stages in the first case is slightly shorter; here, S_C increases proportionally to the increase of the angles until they attain the value of $\pi/3$, after that the graph has a break and the increase becomes curved. We also have an analogous dependence for $\varphi_{01} = \varphi_{02}$; however, the covered distance here is substantially smaller. The time T spent on the passage of the four stages in all three cases increases proportionally to the rotation angles of the links.

We have the following dependences of all these values from the angle θ_0 of the lifting of the end links: the distance S_C does not change with increasing θ_0 , the time T increases proportionally, and the average motion velocity v_{Csr} decreases according to the hyperbolic law.

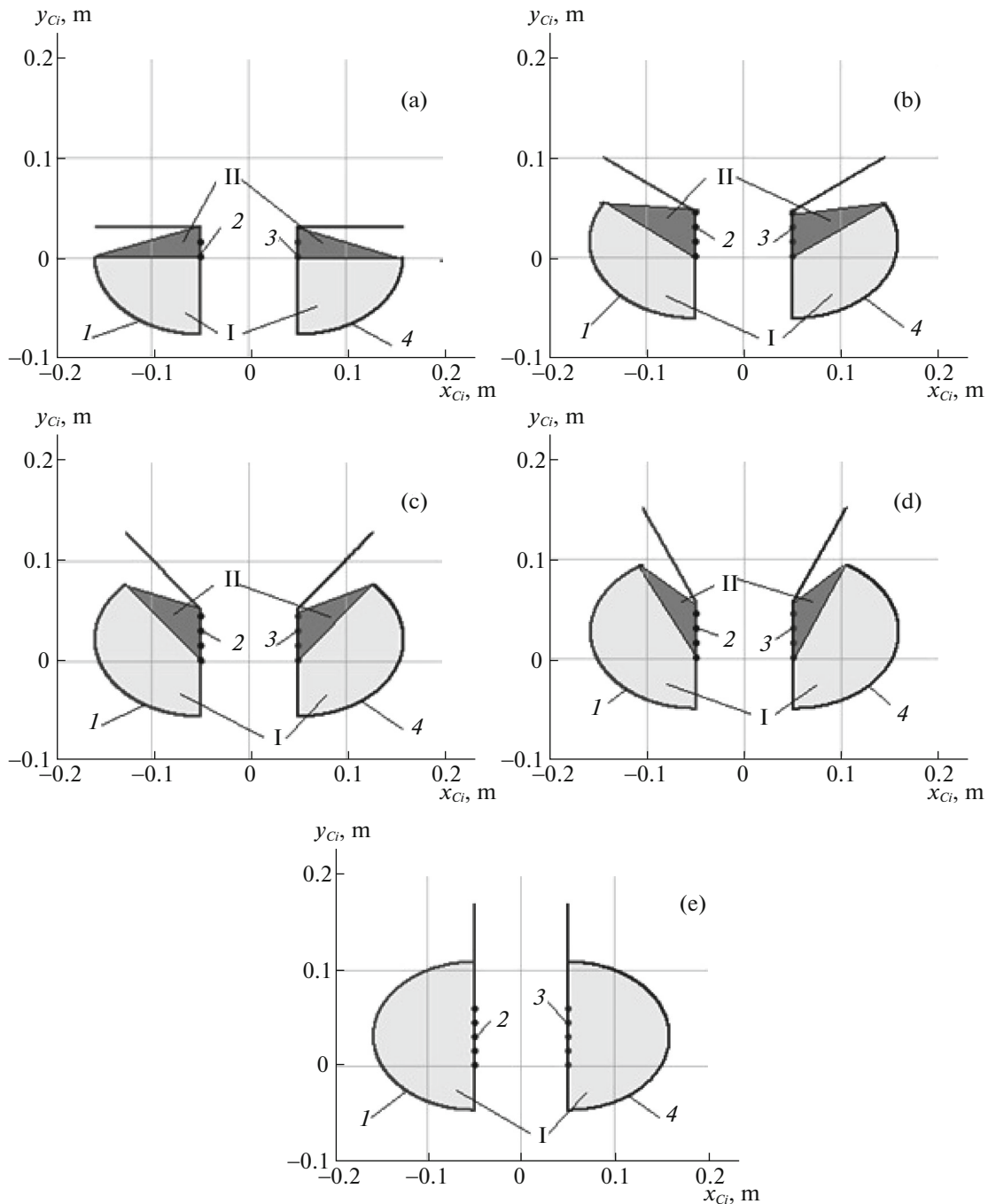


Fig. 18. Areas I and II such that it is impossible to overcome obstacles if they are located in these areas, for $\varphi_{02} = \pi/2$: (a) $\varphi_{01} = 0$, (b) $\varphi_{01} = \pi/6$, (c) $\varphi_{01} = \pi/4$, (d) $\varphi_{01} = \pi/3$, and (e) $\varphi_{01} = \pi/2$.

Figure 17 shows that the average velocity of the robot motion is almost proportional to the amplitude of the moment of the drive that provides the rotation of links 2 and 4 in a horizontal plane. This is caused by the fact that for faster implementation of the first stage, during which link 3 is “ejected” forward along its transverse axis, and for increasing the distance covered by this link, the so-called “fast” movements of links 2 and 4 are required [13–22]. The faster the relative movements of the links the larger the distance covered by link 3 and the shorter the time in which this distance is covered. In this case, the distance S_C increases and the time spent on the passage of the four stages decreases

The amplitude of moment $M_{21\max}$ has an insignificant effect on the average velocity of the robot motion. At first, with the increase of $M_{21\max}$ (up to 0.06 N m), the value of v_{Csr} slightly increases and then

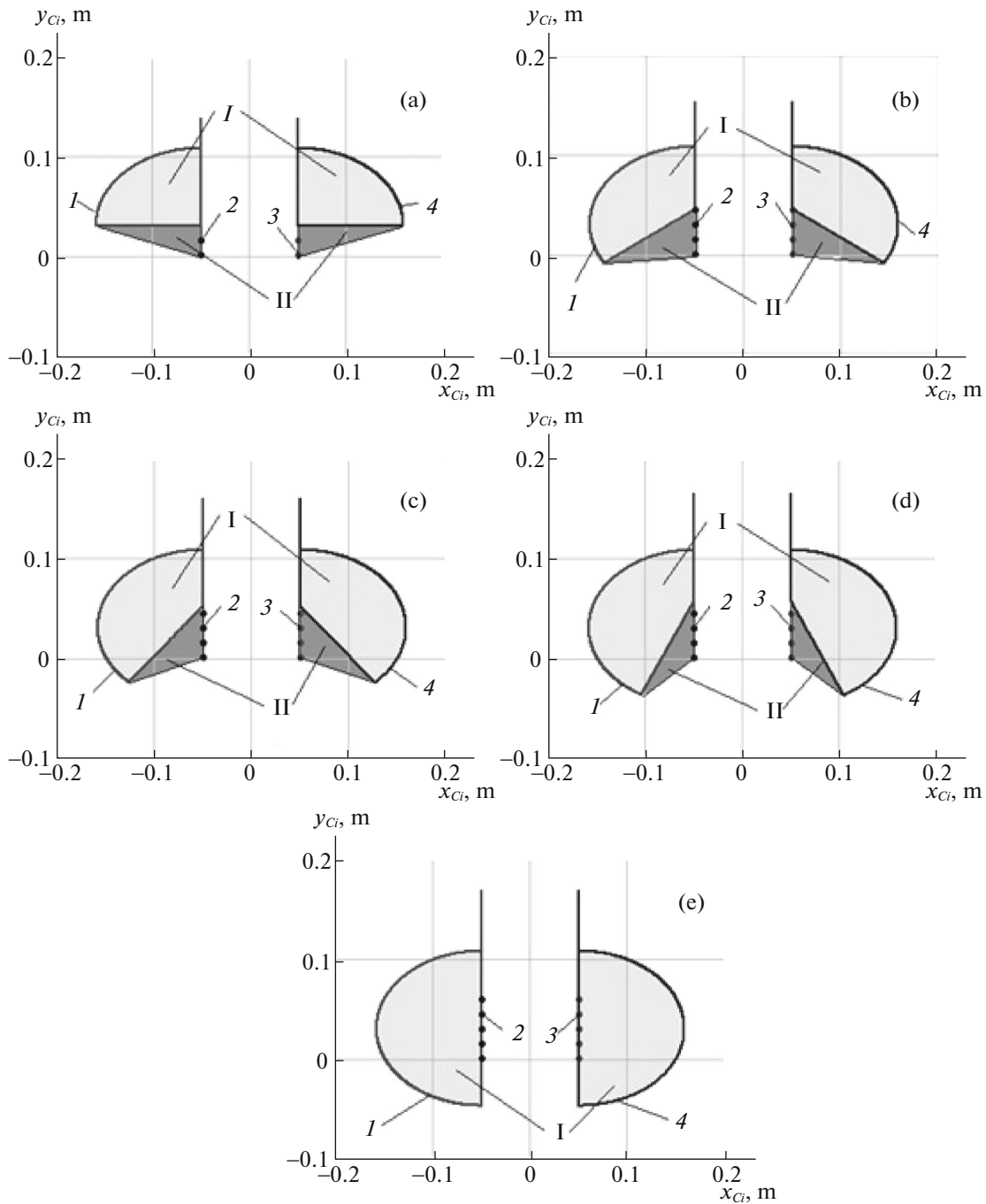


Fig. 19. Areas I and II such that it is impossible to overcome obstacles if they are located in these areas) for $\varphi_{01} = \pi/2$: (a) $\varphi_{02} = 0$, (b) $\varphi_{02} = \pi/6$, (c) $\varphi_{02} = \pi/4$, (d) $\varphi_{02} = \pi/3$, and (e) $\varphi_{02} = \pi/2$.

remains almost fixed; the time of the motion decreases according to the hyperbolic law; and the distance S_C remains unchanged the whole time.

Thus, in order to increase the average velocity of the robot motion, it is necessary to take drives 7 that provide the lateral links' rotation relative to the central link in a horizontal plane, with a large rotation moment, while drives 6 can have a small rotation moment sufficient to move up links 1 and 5 in the vertical planes.

4.3. Investigation of the Robot's Maneuverability

In order to estimate the maneuverability of the device when moving across a plane with obstacles, the criterion of maneuverability ξ is used. With the allowance made for the lengths of the links of the consid-

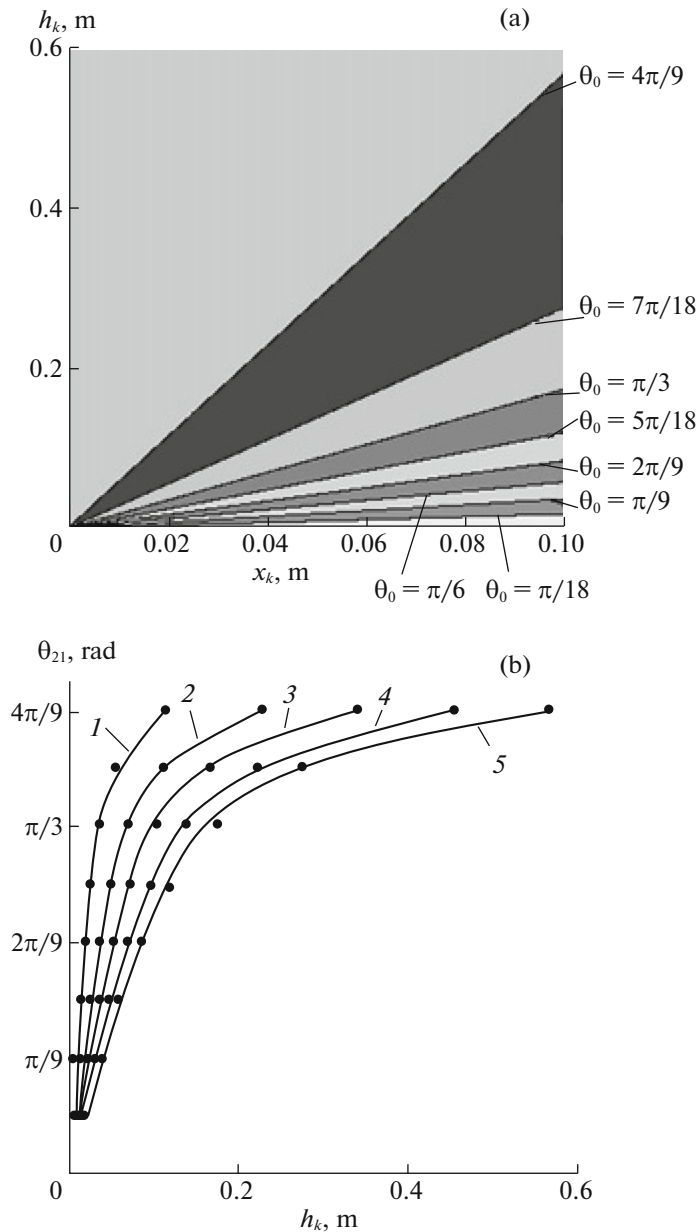


Fig. 20. (a) Level lines of θ_0 in plane $h_k(x_k)$ and (b) graphs of $\theta_0(h_k)$ for (1) $x_k = 0.02 \text{ m}$, (2) $x_k = 0.04 \text{ m}$, (3) $x_k = 0.06 \text{ m}$, (4) $x_k = 0.08 \text{ m}$, and (5) $x_k = 0.1 \text{ m}$.

ered robot, the criterion of maneuverability $\xi = 3.16$ ($L = 316 \text{ mm}$ and $L_{AB\text{min}} = 100 \text{ mm}$); this value is 3.16 times larger than the same criterion in the flat transverse robot motion, where $\xi = 1$, $L = 316 \text{ mm}$, and $L_{AB\text{min}} = 316 \text{ mm}$; i.e., the lifting of links 1 and 5 during the change in the robot's configuration allows one to more than triple the maneuverability of the device.

In addition, we constructed the areas to make it impossible to overcome obstacles if they are located in them; angles φ_{01} and φ_{02} of the rotation of the lateral links in a horizontal plane are used as variable parameters. The graphs in Figs. 18 and 19 show two areas. Area I is bounded by the trajectory of the endpoint of link 1 O_1 at the first stage and the straight line that connects the position of this point at the time of the completion of the first stage with the position of point O_3 at the beginning of this stage (this straight line shows the position of links 1 and 2 at the beginning of the first stage). Area II is bounded by the above-described straight line and the straight line that connects the position of point O_1 at the time of the com-

pletion of the first stage, with the end position of point O_3 at the first stage (this straight line shows the position of links 1 and 2 at the time of the completion of the first stage). In Figs. 18 and 19, the following designations are used: 1 and 4 are the trajectories of points O_1 and O_6 at the first stage and 2 and 3 are the trajectories of points O_3 and O_4 at the first stage.

Here, for $\varphi_{01} = \varphi_{02}$, these areas are symmetrical about the axis that is normal to the direction of the robot motion. The obtained areas are the smallest at small angles φ_{01} and φ_{02} , and largest at $\varphi_{01} = \varphi_{02} = \pi/2$; hence, the robot's maneuverability is improved in the case of moving at small angles of rotation of the lateral links.

Besides, we estimate the effect of the sizes of an obstacle and its location in the plane on the angles of the lifting of the end links. If a considered obstacle has the shape of a parallelepiped, angle θ_0 is acted upon by height h_k of the obstacle and distance x_k to which it is moved from the end point O_3 of link 3 in the direction opposite to the axis of motion. For this purpose, the level lines corresponding to the angles of the lifting of the end links in the plane of parameters h_k and x_k are constructed; these lines demonstrate that the value of angle θ_0 is proportional to both values (see Fig. 20a). The curves in Fig. 20b show that angle θ_0 of the lifting of the end links increases with an increase of the height of an obstacle according to the curvilinear laws; here, with an increase of the distance x_k to which the obstacle is moved from the end point of the central link, the same angle θ_0 will be required at the larger height of the obstacle.

CONCLUSIONS

In this work, we consider one of the modes of moving a five-link crawling robot across a rough plane with discretely located obstacles: the motion along the transverse axis of the central link. The robot differs from analogs by the controlled friction in supports of the central link and the changeable configuration in vertical planes. In order to increase the average motion velocity, the friction coefficients in the supports of the central link varies in such a way that at the stages of changing the configuration of the plant, this link remains stationary on the surface (the friction coefficient is large), whereas in stages of motion the considered link moves in a given direction (the friction coefficient is small). To improve the maneuverability in overcoming obstacles without contact, the device structurally possesses the property of detaching the end links from a surface; this reduces the minimum distances between obstacles at the same transverse size of the robot and allows the robot to overcome obstacles that are spaced more densely. The design scheme of the robot is developed and the sequence of the stages of its motion is proposed; for each step, systems of differential equations are written with allowance made for the restrictions applied on the plant and for the conditions of switching between them, an automatic control system of the robot motion is designed, and operation algorithms of the logical controller are presented. Besides, considerable attention is paid to the robot's contactless passage between obstacles.

As a result of the simulation by the numerical method, the graphs of the time dependences of, first, the coordinates for the centers of mass of the links, second, the rotation angles, and, third, the angular velocities are obtained; these graphs allow one to test the operation of the software package and study the features of the movement of the robot's links at each stage.

In addition, the dependences of the average velocity of the device's motion on the control parameters are presented. It is found that in order to increase this velocity, it is necessary to implement the plant's motion with small angles φ_{01} and φ_{02} of the rotation of the links in a horizontal plane (no larger than $4\pi/9$); with minimum possible angles θ_0 of the lifting of the end links; with the largest amplitudes of the moments $M_{32\max}$ ($M_{34\max}$), which provide the rotations of the lateral links relative to the central link in a horizontal plane; and with amplitudes of the moments $M_{21\max}$ ($M_{45\max}$), which lift the end links, close to the minimum amplitudes.

We also estimated the maneuverability of the device that moves across a surface with discretely located obstacles. For this purpose, the criterion ξ is introduced, which represents the ratio of the largest transverse dimension of the robot to the minimum distance between obstacles. It is found that the change in the robot's configuration due to the lifting of the end links more than triples its maneuverability. As a result of the simulation, areas of the surface are found such that it is impossible to overcome obstacles without contact if they are located in these areas. In addition, it is found that these areas are expanded with a decrease of angles φ_{01} and φ_{02} . Besides, a correspondence is established between the minimum required angle of the lifting of the end links θ_0 and the size of an obstacle, together with its location in the plane.

ACKNOWLEDGMENTS

This work was financially supported by the Russian Foundation for Basic Research (project no. 15-51-12381) and the Russian Science Foundation (project no. 14-39-00008).

REFERENCES

1. T. Tanaka, K. Harigaya, and T. Nakamura, "Development of a peristaltic crawling robot for long-distance inspection of sewer pipes," in *Proceedings of the IEEE/ASME International Conference on Advanced Intelligent Mechatronics AIM, Besançon, France, July 8–11, 2014*.
2. S. Jatsun, O. Loktionova, and A. Malchikov, "Six-link in-pipe crawling robot," in *Advances on Theory and Practice of Robots and Manipulators* (Springer International, New York, 2014), pp. 341–348.
3. A. Houssam, A. Ananiev, and I. Kalaykov, "Stability study of underwater crawling robot on non-horizontal surface," in *Proceedings of the 17th International Conference on Climbing and Walking Robots CLAWAR, Poznan, Poland, 2014*.
4. E. S. Conkur and R. Gurbuz, "Path planning algorithm for snake-like robots," *Inform. Technol. Control*, **37**, 159–162 (2008).
5. D. Lounis, D. Spinello, W. Gueaieb, and H. Sarfraz, "Planar kinematics analysis of a snake-like robot," *Robotica*, **32**, 659–675 (2014).
6. W. Wu, X. Jun, Y. H. L. Wei, S. M. Ri, X. C. Chun, Y. H. Zhen, and L. Zhong, "Structure design of climbing snake-like robot for detection of cable-stayed bridge," *Appl. Mech. Mater.* **598**, 610–618 (2014).
7. T. Matsuo and K. Ishii, "Adaptative motion control system of a snake-like robot using a neural oscillator network," in *Proceedings of the Joint 7th International Conference on Soft Computing and Intelligent Systems SCIS, and 15th International Symposium on Advanced Intelligent Systems ISIS, Abu Dhabi, 2014*.
8. L. Yan-hui, L. Li, W. Ming-hui, and G. Xian, "Simulation study on serpentine locomotion of underwater snake-like robot," *Int. J. Control Automat.*, **8**, 373–384 (2015).
9. G. Li, W. Li, J. Zhang, and H. Zhang, "Analysis and design of asymmetric oscillation for caterpillar-like locomotion," *J. Bionic Eng.*, **12**, 190–203 (2015).
10. G. Li, H. Zhang, J. Zhang, and R. T. Bye, "Development of adaptive locomotion of a caterpillar-like robot based on a sensory feedback CPG model," *Adv. Robotics*, **28**, 389–401 (2014).
11. S. Gorges, C. Riehs, and K. Zimmermann, T. Kästner, "A cascaded worm-like locomotion system – constructive design, software and experimental environment," in *Proceedings of the 58th Ilmenau Scientific Colloquium, Ilmenau, 2014*.
12. S. Jatsun and A. Malchikov, "Mobile worm-like robots for pipe inspection," in *Handbook of Research on Advancements in Robotics and Mechatronics* (Am. Univ. in Cairo, Egypt, 2014), pp. 168–218.
13. F. L. Chernous'ko, "On motion of a three-link mechanism along a horizontal plane," *Prikl. Mat. Mekh.*, **65**, 15–20 (2001).
14. F. L. Chernous'ko, "Controllable motions of a two-link mechanism along a horizontal plane," *J. Appl. Math. Mech.*, **65**, 565–577 (2001).
15. F. L. Chernous'ko, "Motion of multilink mechanisms along a plane," in *Problems of Mechanics, Collection of Articles Dedicated to 90 Years from A. Yu. Ishlinskii Birthday* (Fizmatlit, Moscow, 2003), pp. 783–802.
16. F. L. Chernous'ko, "Wave-like motion of multilink mechanism along a horizontal plane," *Prikl. Mat. Mekh.*, **64**, 518–531 (2000).
17. F. L. Chernous'ko, "Motion of flat multilink mechanism along a horizontal plane," *Prikl. Mat. Mekh.*, **64**, 8–18 (2000).
18. F. L. Chernous'ko, "The motion of a flat linkage over a horizontal plane," *Dokl. Phys.*, **45**, 42 (2000).
19. F. L. Chernous'ko, "Optimal control of the motion of a multilink system in a resistive medium," *J. Appl. Math. Mech.*, **76**, 255–267 (2012).
20. F. L. Chernous'ko and M. M. Shunderyuk, "The influence of friction forces on the dynamics of a two-link mobile robot," *J. Appl. Math. Mech.*, **74**, 13–23 (2010).
21. F. L. Chernous'ko, "Optimal move of a multilink system in a resistive medium," *Tr. IMM UrO RAN* **17** (2), 240–255 (2011).
22. F. L. Chernous'ko, "Control of multilink mechanisms motion on rough plane," *Tr. IMM UrO RAN* **6** (1), 277–287 (2000).
23. S. A. Bashkurov, "Motion control algorithms and simulation of the dynamics of multilink robots moving based on the principles of a traveling wave," *J. Comput. Syst. Sci. Int.*, **46**, 162 (2007).
24. K. S. Sorokin, "Control of a three-link robot moving on the plane with friction," *J. Comput. Syst. Sci. Int.*, **48**, 489 (2009).
25. N. A. Sobolev and K. S. Sorokin, "Experimental investigation of snakelike motions of a three-link mechanism," *J. Comput. Syst. Sci. Int.*, **45**, 841 (2006).

26. S. F. Yatsun, L. Yu. Volkova, G. S. Naumov, and A. S. Yatsun, "Modelling of movement of the three-link robot with operated friction forces on the horizontal surface," in *Proceedings of the 16th International Conference on Climbing and Walking Robots and the Support Technologies for Mobile Machines, Sydney, 2013*, pp. 677–684.
27. L. Yu. Vorochaeva, G. S. Naumov, and S. F. Yatsun, "Simulation of motion of a three-link robot with controlled friction forces on a horizontal rough surface," *J. Comput. Syst. Sci. Int.* **54**, 151–164 (2015).
28. S. F. Yatsun, L. Yu. Volkova, S. B. Rublev, and G. S. Naumov, "Three-link creeping robot as a vehicle," in *Progress of Vehicles and Transport Systems* (Volgogr. Gos. Tekh. Univ., Volgograd, 2013), pp. 293–294 [in Russian].
29. S. F. Yatsun, V. Ya. Mishchenko, and G. S. Naumov, "Creeping mobile robot," RF Patent No. 2567944, *Byull. Izobret.* No. 31 (2015).
30. S. F. Yatsun, L. Yu. Volkova, and G. S. Naumov, "Software for calculation of the motion parameters of three-link mechanism during transverse gait," State Registration Certificate of Computer Software No. 2014611745 (2014).
31. S. F. Yatsun, L. Yu. Volkova, and G. S. Naumov, "Software for calculation of the motion parameters of three-link mechanism during longitudinal gait," State Registration Certificate of Computer Software No. 2014611746 (2014).
32. S. F. Yatsun, L. Yu. Vorochaeva, A. S. Yatsun, and A. V. Malchikov, "Theoretical and experimental studies of transverse dimensional gait of five-link mobile robot on rough surface," in *Proceedings of the 10th International Symposium on Mechatronics and Its Applications ISMA'15, Istanbul, 2015*, p. 35.
33. N. Bolotnik, M. Pivovarov, I. Zeidis, and K. Zimmermann, "Dynamics and control of a two-module mobile robot on a rough surface," in *Advances on Theory and Practice of Robots and Manipulators* (Springer International, New York, 2014), pp. 141–148.
34. M. H. P. Dekker, *Zero-Moment Point Method for Stable Biped Walking* (Univ. of Technology, Eindhoven, 2009).
35. M. Vukobratovic and B. Borovac, "Zero—moment point—thirty five years of its life," *Int. J. Humanoid Robotics* **1**, 157–173 (2004).
36. L. Yu. Volkova, I. V. Lupekhina, G. Ya. Panovko, and S. F. Yatsun, "Dynamics of the vibration driven tool at its interaction with the processing material," *Mashinostr. Inzhen. Obrazov.*, No. 4, 63–72 (2010).

Translated by L. Kartvelishvili